

# Estimating Covariance Matrices for Two- and Three-Point Correlation Function Moments in Arbitrary Survey Geometries

Oliver H. E. Philcox<sup>1,2\*</sup> and Daniel J. Eisenstein<sup>1</sup>

<sup>1</sup>*Center for Astrophysics | Harvard & Smithsonian, 60 Garden St., MA 02138, USA*

<sup>2</sup>*Department of Astrophysical Sciences, Princeton University, Princeton, NJ 08544, USA*

Accepted 2019 October 9. Received 2019 September 24; in original form 2019 June 19

## ABSTRACT

We present configuration-space estimators for the auto- and cross-covariance of two- and three-point correlation functions (2PCF and 3PCF) in general survey geometries. These are derived in the Gaussian limit (setting higher-order correlation functions to zero), but for arbitrary non-linear 2PCFs (which may be estimated from the survey itself), with a shot-noise rescaling parameter included to capture non-Gaussianity. We generalize previous approaches to include Legendre moments via a geometry-correction function calibrated from measured pair and triple counts. Making use of importance sampling and random particle catalogs, we can estimate model covariances in fractions of the time required to do so with mocks, obtaining estimates with negligible sampling noise in  $\sim 10$  ( $\sim 100$ ) CPU-hours for the 2PCF (3PCF) auto-covariance. We compare results to sample covariances from a suite of BOSS DR12 mocks and find the matrices to be in good agreement, assuming a shot-noise rescaling parameter of 1.03 (1.20) for the 2PCF (3PCF). To obtain strongest constraints on cosmological parameters we must use multiple statistics in concert; having robust methods to measure their covariances at low computational cost is thus of great relevance to upcoming surveys.

**Key words:** methods: statistical, numerical – Cosmology: large-scale structure of Universe, theory – galaxies: statistics

## 1 INTRODUCTION

In the standard cosmological paradigm, where density fluctuations are created in reheating following inflation, the primordial over-density field,  $\delta$ , is expected to be Gaussian and thus describable completely by its (isotropic) power spectrum, or associated two-point correlation function (2PCF),  $\xi(r)$ . During the later evolution of the Universe, gravitational effects introduce non-Gaussianities into  $\delta$ , implying that higher-order statistics are required to fully describe the field, the prime candidate being the isotropic three-point correlation function (3PCF) (see [Bernardeau et al. \(2002\)](#) and [Szapudi \(2005\)](#) for reviews). There is a wealth of research concerning both the expected forms of the configuration-space 3PCF (e.g. [Bernardeau et al. 2002](#); [Sefusatti et al. 2006](#); [Marín et al. 2008](#); [Slepian & Eisenstein 2017](#); [Yuan et al. 2017, 2018](#)) and estimators for its measurement (e.g. [Szapudi & Szalay 1998](#); [Moore et al. 2001](#); [Gray et al. 2004](#); [Szapudi 2004](#); [Nichol et al. 2006](#); [Slepian & Eisenstein 2015b](#)), and it has been shown that this observable is able to break degeneracies between cosmic parameters (e.g. [Gaztanaga & Frieman 1994](#); [Frieman & Gaztanaga 1994](#); [Jing & Börner 2004](#); [Guo et al. 2015](#)) and provide probes of primordial non-Gaussianity ([Desjacques & Seljak 2010](#)). Because of this, the isotropic 3PCF has become a powerful addition to the analyst’s toolkit, and has been used in a number of analyses (e.g. [Kayo et al. 2004](#); [Jing & Börner 2004](#); [Marín 2011](#); [Slepian et al. 2015, 2017, 2018](#)).

Despite the Universe’s statistical isotropy, the measured 2PCF and 3PCF are far from isotropic, both due to Redshift Space Distortions (RSD), caused by degeneracies between cosmic and peculiar velocity redshifts, and the Alcock-Paczynski effect, where anisotropy is introduced due to incorrectly assumed cosmology ([Alcock & Paczynski 1979](#)). In particular, the

\* E-mail: [ohp2@alumni.cam.ac.uk](mailto:ohp2@alumni.cam.ac.uk)

Finger-of-God (Kaiser) effect boosts (reduces) the power parallel to the line of sight (LoS), resulting in a LoS-dependent correlation function (Jackson 1972; Kaiser 1987). Naïvely, this may seem to be simply an irritation, yet in practice anisotropy provides an independent probe of structure formation, tightening the constraints on cosmological parameters. Due to RSD, the 2PCF becomes a two-dimensional function  $\xi(r, \mu)$ , where  $\mu$  is the angle of a pair of galaxies to the LoS, whilst the 3PCF now depends on an additional two parameters describing the orientation of the triangle of galaxies to the LoS (Scoccimarro et al. 1999). Due to the high dimensionality of the anisotropic 3PCF, its measurements are inherently noisy, thus, despite there existing a multitude of algorithms for its estimation (e.g. Zhang & Pen 2005; Gardner et al. 2007; Slepian & Eisenstein 2018), it has been seldom used in cosmological analyses thus far. In contrast, the anisotropic 2PCF is a widely adopted quantity, commonly presented in one of two forms; (a) in  $(r, \mu)$ -space wedges (recent examples being Kazin et al. 2012 and Sánchez et al. 2017) or (b) decomposed into Legendre moments  $\xi_\ell(r)$  (recently Satpathy et al. 2017). The latter form is particularly useful since most information is captured by the first few (even) multipoles, obviating the need for a large number of (noisy) angular bins.

To constrain cosmological parameters, we must compare the above statistics to established models, requiring good understanding of the covariance matrices of our measurements. Furthermore, stronger parameter bounds are obtained by using multiple statistics (e.g. both the 2PCF and 3PCF), with optimal analyses requiring full knowledge of the *cross-covariance* matrices. Any such covariance is relatively easy to derive for uniform periodic simulation boxes (e.g. see Sugiyama et al. (2019) for perturbation theory covariances in Fourier space), yet the selection functions of realistic surveys are far from simple, with power on a range of scales due to effects such as non-uniform boundaries and fiber collisions. The survey geometry has a significant impact on the output covariances, thus ignoring it will lead to distortions in parameter error bars. To account for this, covariance matrices are usually computed using a set of ‘mock’ catalogs created with the same selection functions as the observational data. Creating high-fidelity mock catalogs is computationally expensive, especially since we require a large number of mocks to avoid noise in the covariance matrices biasing the derived parameter error bars (Taylor et al. 2013; Dawson et al. 2013; Percival et al. 2014). In addition, future surveys (e.g. Euclid (Laureijs et al. 2011), DESI (Levi et al. 2013) and WFIRST (Spergel et al. 2015)) will perform tomographic analyses, greatly increasing the number of correlation function bins, thus requiring far more mocks for the same level of covariance matrix noise. Approximate methods for covariance generation can partially alleviate this problem; these permit fast estimation of low-noise matrices, allowing us to create fewer mocks of higher quality, which remain important for analysis of systematics.

In O’Connell et al. (2016), it was shown that the 2PCF covariance matrix for an arbitrary survey geometry could be written as a sum of configuration-space integrals (similar to Bernstein 1994), and quickly evaluated using importance sampling techniques. Although the basic formalism assumes Gaussianity, good agreement of theoretical and mock-based covariances was found using a few percent rescaling of the shot-noise amplitude, calibrated either from a small suite of mocks, or from the survey itself via jackknives (O’Connell & Eisenstein 2019). The formalism was further developed in Philcox et al. (2019), where a new algorithm was introduced, `RascalC`,<sup>1</sup> allowing for single- and multi-tracer 2PCF covariances to be computed from a single survey in a fraction of the previous computation time. Our goal in this work is to extend the previous formalism to more complex cases; the auto- and cross-covariance matrices of anisotropic 2PCF and isotropic 3PCF Legendre moments. We introduce a geometry-correction function to allow for moments to be computed directly (rather than in post-processing) and demonstrate that our output precision matrices are in good agreement with those from simulations. Via efficient importance sampling methods we are able to produce 2PCF (3PCF) auto-covariance matrices with negligible sampling noise in  $\sim 10$  ( $\sim 100$ ) CPU-hours.

This paper is structured as follows. We begin with an overview of previous 2PCF estimators and covariances in Sec. 2, before discussing the extension to the covariance of the Legendre moments of single- and multi-field 2PCFs in Sec. 3, along with validation using BOSS DR12 simulations. Sec. 4 describes the 3PCF estimator adopted herein, before its theoretical covariance, and cross-covariance with the 2PCF, is considered in Sec. 5, along with application to BOSS DR12 mocks. We conclude with a summary and discussion in Sec. 6, with a useful theoretical result presented in appendix A.

## 2 OVERVIEW OF PREVIOUS WORK

We begin by summarizing the estimators for the 2PCF and the formalism for the covariance matrices, as in O’Connell et al. (2016), O’Connell & Eisenstein (2019) and Philcox et al. (2019), with slightly modified notation. For a galaxy survey measuring a total of  $N_{\text{gal}}$  galaxies with continuous (mean) number density and weight functions  $n(\mathbf{r})$  and  $w(\mathbf{r})$ , we may define the anisotropic 2PCF as a ratio of pair counts

$$\hat{\xi}(r, \mu) = \frac{NN(r, \mu)}{RR(r, \mu)} \quad (2.1)$$

<sup>1</sup> This has been extended to include the Legendre-binned 2PCF and 3PCF auto-covariances discussed in this paper. Full documentation is provided at [RascalC.readthedocs.io](https://github.com/philcox/RascalC.readthedocs.io).

(Landy & Szalay 1993), where  $\mu = \cos\theta$  measures the angular coordinate (using symmetry to restrict to  $\mu \in [0, 1]$ ) and  $N = (D - R)$ , with  $D$  and  $R$  representing galaxies and random particles respectively. In some radial bin  $a$  and angular bin  $c$ , the 2PCF estimate becomes

$$\hat{\xi}_c^a = \frac{NN_c^a}{RR_c^a} \quad (2.2)$$

where  $NN_c^a$  and  $RR_c^a$  are defined by

$$\begin{aligned} NN_c^a &= \sum_{i \neq j} n_i n_j w_i w_j \Theta^a(r_{ij}) \Theta^c(\mu_{ij}) \delta_i \delta_j \\ RR_c^a &= \sum_{i \neq j} n_i n_j w_i w_j \Theta^a(r_{ij}) \Theta^c(\mu_{ij}), \end{aligned} \quad (2.3)$$

(for  $X_i \equiv X(\mathbf{r}_i)$ ), dividing the survey into small cubic boxes which contain at most one galaxy and summing. Here  $\delta_i$  is the fractional galaxy overdensity in cell  $i$ ,  $\mu_{ij}$  is the angle between the vector  $\mathbf{r}_i - \mathbf{r}_j$  and the LoS (or the  $z$ -axis for a cuboidal simulation), and the binning functions  $\Theta^a(Y)$  are unity if  $Y$  is in the bin  $a$  and zero else. Unlike in previous works, we expand the binning function into a radial and angular part, for later convenience. Equivalently, the pair counts may be written in continuous form;

$$\begin{aligned} NN_c^a &= \int d^3 \mathbf{r}_i d^3 \mathbf{r}_j n(\mathbf{r}_i) n(\mathbf{r}_j) w(\mathbf{r}_i) w(\mathbf{r}_j) \Theta^a(|\mathbf{r}_i - \mathbf{r}_j|) \Theta^c(\mu_{(\mathbf{r}_i - \mathbf{r}_j)}) \delta(\mathbf{r}_i) \delta(\mathbf{r}_j) \\ RR_c^a &= \int d^3 \mathbf{r}_i d^3 \mathbf{r}_j n(\mathbf{r}_i) n(\mathbf{r}_j) w(\mathbf{r}_i) w(\mathbf{r}_j) \Theta^a(|\mathbf{r}_i - \mathbf{r}_j|) \Theta^c(\mu_{(\mathbf{r}_i - \mathbf{r}_j)}). \end{aligned} \quad (2.4)$$

Given the 2PCF estimator, we define the covariance matrix  $C_{cd}^{ab}$  in radial bins  $(a, b)$  and  $\mu$ -bins  $(c, d)$  as

$$\begin{aligned} \text{cov}(\hat{\xi}_c^a, \hat{\xi}_d^b) &\equiv C_{cd}^{ab} = \langle \hat{\xi}_c^a \hat{\xi}_d^b \rangle - \langle \hat{\xi}_c^a \rangle \langle \hat{\xi}_d^b \rangle \\ &= \frac{1}{RR_c^a RR_d^b} \sum_{i \neq j} \sum_{k \neq l} n_i n_j n_k n_l w_i w_j w_k w_l \Theta^a(r_{ij}) \Theta^c(\mu_{ij}) \Theta^b(r_{kl}) \Theta^d(\mu_{kl}) [\langle \delta_i \delta_j \delta_k \delta_l \rangle - \langle \delta_i \delta_j \rangle \langle \delta_k \delta_l \rangle], \end{aligned} \quad (2.5)$$

inserting the expanded 2PCF estimator. In O'Connell et al. (2016), it was shown that this could be expanded into 2-, 3- and 4-point summations using the relation

$$\sum_{i \neq j} \sum_{k \neq l} X_{ij} Y_{kl} = \sum_{i \neq j \neq k \neq l} X_{ij} Y_{kl} + 4 \sum_{i \neq j \neq k} X_{ij} Y_{kj} + 2 \sum_{i \neq j} X_{ij} Y_{ij} \quad (2.6)$$

for summands  $X_{ij}$  and  $Y_{kl}$  symmetric under  $i \leftrightarrow j$  and  $k \leftrightarrow l$  interchanges. To expand out the expectation terms, we apply the shot-noise approximation

$$\delta_i^2 \approx \frac{\alpha}{n_i} (1 + \delta_i) \quad (2.7)$$

(including a shot-noise rescaling factor  $\alpha$  to capture non-Gaussianity as discussed below) and Isserlis' (Wick's) theorem (Isserlis 1918) giving

$$\begin{aligned} \langle \delta_i \delta_j \delta_k \delta_l \rangle - \langle \delta_i \delta_j \rangle \langle \delta_k \delta_l \rangle &= \xi_{ijkl}^{(4)} + \xi_{ik} \xi_{jl} + \xi_{il} \xi_{jk} \\ \langle \delta_i \delta_j \delta_k \delta_j \rangle &\approx \frac{\alpha}{n_j} \langle (1 + \delta_j) \delta_i \delta_k \rangle = \frac{\alpha}{n_i} (\zeta_{ijk} + \xi_{ik}) \\ \langle \delta_i \delta_j \delta_i \delta_j \rangle &\approx \frac{\alpha^2}{n_i n_j} \langle (1 + \delta_i) \delta_j \delta_k \rangle = \frac{\alpha^2}{n_i n_j} (1 + \xi_{ij}), \end{aligned} \quad (2.8)$$

where  $\zeta$  and  $\xi^{(4)}$  are the three- and four-point connected correlation functions. Inserting Eqs. 2.6 & 2.8 into Eq. 2.5 gives the full covariance

$$C_{cd}^{ab} = 4 C_{cd}^{ab} + \alpha \times 3 C_{cd}^{ab} + \alpha^2 \times 2 C_{cd}^{ab} \quad (2.9)$$

with the definitions

$$\begin{aligned} 4 C_{cd}^{ab} &= \frac{1}{RR_c^a RR_d^b} \sum_{i \neq j \neq k \neq l} n_i n_j n_k n_l w_i w_j w_k w_l \Theta^a(r_{ij}) \Theta^c(\mu_{ij}) \Theta^b(r_{kl}) \Theta^d(\mu_{kl}) [\xi_{ijkl}^{(4)} + 2 \xi_{ik} \xi_{jl}] \\ 3 C_{cd}^{ab} &= \frac{4}{RR_c^a RR_d^b} \sum_{i \neq j \neq k} n_i n_j n_k w_i (w_j)^2 w_k \Theta^a(r_{ij}) \Theta^c(\mu_{ij}) \Theta^b(r_{jk}) \Theta^d(\mu_{jk}) [\zeta_{ijk} + \xi_{ik}] \\ 2 C_{cd}^{ab} &= \frac{2 \delta^{ab} \delta^{cd}}{RR_c^a RR_d^b} \sum_{i \neq j} n_i n_j (w_i w_j)^2 \Theta^a(r_{ij}) \Theta^c(\mu_{ij}) [1 + \xi_{ij}] \end{aligned} \quad (2.10)$$

(cf. O'Connell et al. 2016, Eqs. 2.15-2.18), where  $\delta^{ab}$  and  $\delta^{cd}$  are Kronecker deltas. As in Philcox et al. (2019), we have replaced  $\xi_{ik} \xi_{jl} + \xi_{il} \xi_{jk}$  with  $2 \xi_{ik} \xi_{jl}$  in the 4-point integral, exploiting the relabelling symmetries of the summand. In previous work, we take the Gaussian limit, setting all higher-order correlation functions to zero, such that only the Gaussian (yet non-linear)

2PCF  $\xi_{ij}$  is used in the above expressions, with shot-noise rescaling (i.e.  $\alpha > 1$ ) used to encapsulate the higher-point effects. In the expressions above, we include all terms for clarity, and note that these may be translated into continuous form by replacing  $\sum_i \rightarrow \int d^3\mathbf{r}_i$  and promoting quantities to be continuous functions of the spatial position  $\mathbf{r}$  e.g.  $n_i \rightarrow n(\mathbf{r}_i)$  and  $\xi_{ij} \rightarrow \xi(\mathbf{r}_i - \mathbf{r}_j)$ .

Before extending these techniques further, it is worth pausing to consider our main assumption, that non-Gaussianity can be well approximated using a rescaling of galactic shot-noise. This is motivated by noting that the principal action of the higher-point correlation function terms (that source non-Gaussianity) is to provide additional clustering power at small distances, usually less than the covariance binning width. By artificially increasing the level of shot-noise, we boost the clustering on *infinitesimally* small scales, which is found to be a fair approximation in practice. The non-Gaussian covariance matrix terms depend on integrals of the higher-point correlation functions; our assumption is equivalent to replacing these with their contractions, giving terms identical in form to those from shot-noise. Mathematically, this is a good approximation if we assume the correlation functions to be dominated by their squeezed limits on the relevant scales. Whether shot-noise rescaling adequately describes non-Gaussianity is uncertain *a priori*, but previous works (O’Connell et al. 2016; O’Connell & Eisenstein 2019; Philcox et al. 2019) have demonstrated excellent agreement between the theoretical covariances and those of large suites of mocks, as well as the shown the method’s utility in BAO-scale analyses (Vargas-Magaña et al. 2018).

### 3 TWO POINT FUNCTION COVARIANCES IN LEGENDRE POLYNOMIAL BINS

#### 3.1 Legendre Moment Estimator for the 2PCF

In previous works the anisotropic 2PCF has been assumed to be measured as a function of the angular coordinate  $\mu$ , yet in many analyses (e.g. Peacock et al. 2001; DESI Collaboration et al. 2016; Alam et al. 2017; Sánchez et al. 2017; Zarrouk et al. 2018) it is presented instead in terms of its Legendre moments  $\xi_\ell(r)$ , which can be simply related to the power spectrum multipoles. Conversion between  $\xi_\ell(r)$  and  $\xi(r, \mu)$  is achieved via the standard relation

$$\xi(r, \mu) = \sum_{\ell=0}^{\infty} \xi_\ell(r) L_\ell(\mu) \quad (3.1)$$

where  $L_\ell(\mu)$  is the Legendre polynomial of order  $\ell$ . Although this provides a way to convert from angularly-binned 2PCF estimates to Legendre moments, it is much more efficient to compute the latter quantities directly, avoiding errors from finite  $\mu$  binning and the necessity for a finely binned  $\xi(r, \mu)$ . Via completeness of the Legendre polynomials (i.e.  $\int_{-1}^1 d\mu L_\ell(\mu) L_{\ell'}(\mu) = 2\delta_{\ell\ell'}/(2\ell+1)$ ), the above relation may be inverted to yield

$$\xi_\ell(r) = \frac{2\ell+1}{2} \int_{-1}^1 d\mu \xi(r, \mu) L_\ell(\mu) = \frac{(-1)^\ell + 1}{2} (2\ell+1) \int_0^1 d\mu \xi(r, \mu) L_\ell(\mu) \quad (3.2)$$

using  $\xi(r, \mu) = \xi(r, -\mu)$  and the symmetry properties of  $L_\ell(\mu)$ . From the prefactor, we note that all odd  $\ell$  terms vanish, thus we restrict to even  $\ell$  henceforth, using a total of  $N_\ell = \ell_{\max}/2 + 1$  bins. Restricting to a radial bin  $a$  (with  $r \in [r_{a,\min}, r_{a,\max}]$  and center  $r_a$ ) this becomes

$$\xi_\ell^a = (2\ell+1) \int_0^1 d\mu \xi^a(\mu) L_\ell(\mu). \quad (3.3)$$

where the function  $\xi^a(\mu)$ , binned only in the radial coordinate, is defined by the reduced Landy-Szalay estimator

$$\hat{\xi}^a(\mu) = \frac{NN^a(\mu)}{RR^a(\mu)} \quad (3.4)$$

as before (Eqs. 2.1 & 2.2). The quantities  $XX^a(\mu)$  (for  $X \in \{D, R\}$ ) may be identified with pair-counts in vanishingly small angular bins  $\{c\}$  via

$$XX_c^a = \int d\mu XX^a(\mu) \Theta^c(\mu) \approx XX^a(\mu_c) \delta\mu \quad (3.5)$$

where  $\mu_c$  is the center of bin  $c$  with width  $\delta\mu$ . This becomes exact in the limit  $\delta\mu \rightarrow 0$ . This may be inverted to yield

$$XX^a(\mu) \approx \sum_c \frac{XX_c^a}{\delta\mu} \Theta^c(\mu) \quad (3.6)$$

To proceed, we require an analytic form for the  $RR$  pair counts. For a uniform infinite survey, the continuous form of  $RR_c^a$  (Eq. 2.4) may be rewritten as

$$RR_c^a = (nw)^2 \int d^3\mathbf{r}_i d^3\mathbf{r}_j \Theta^a(|\mathbf{r}_i - \mathbf{r}_j|) \Theta^c(\mu_{(\mathbf{r}_i - \mathbf{r}_j)}) \quad (3.7)$$

since  $n$  and  $w$  will be independent of position. Substituting  $\mathbf{x} = \mathbf{r}_i - \mathbf{r}_j$  gives

$$\begin{aligned} RR_c^a &= (nw)^2 \left[ \int d^3 \mathbf{r}_j \right] \left[ \int d^3 \mathbf{x} \Theta^a(|\mathbf{x}|) \Theta^c(\mu_x) \right] \\ &= (nw)^2 \times V \times \int x^2 dx \Theta^a(x) \times \int_0^{2\pi} d\phi_x \times \int_{-1}^1 d\mu_x \Theta^c(\mu_x) \\ &\approx (nw)^2 \times V \times \frac{1}{3} \left( r_{a,\max}^3 - r_{a,\min}^3 \right) \times 2\pi \times 2\delta\mu \end{aligned} \quad (3.8)$$

defining  $V$  as the survey volume and noting that an additional factor of 2 arises in the  $\mu$  binning, since we do not distinguish between positive and negative  $\mu$ . Similar to Xu et al. (2010), we introduce a *survey correction factor*  $\Phi(r_a, \mu)$  for each radial bin  $a$  to encapsulate the effects of non-uniform sampling and the survey boundaries, defining

$$RR^a(\mu) \equiv \frac{\frac{4\pi}{3} V \overline{(nw)^2} \left( r_{a,\max}^3 - r_{a,\min}^3 \right)}{\Phi(r_a, \mu)} \quad (3.9)$$

(converting to continuous form in  $\mu$  via Eq. 3.5), where  $\overline{(nw)^2}$  is the survey-averaged value of  $(nw)^2$ . In Xu et al. (2010), the associated function  $\Phi(r, \mu)$  (continuous in both  $r$  and  $\mu$ ) was shown to be well approximated by a smooth two-dimensional function; here we may use a distinct function for each radial bin, computed by fitting the ratio of our infinite model and empirically derived pair counts, e.g. from `corrfunc`<sup>2</sup> (Sinha & Garrison 2017). In the case of an infinite survey we expect  $\Phi(r_a, \mu) = 1$  for all  $(r_a, \mu)$ , though in real surveys stronger departures from  $\Phi = 1$  are expected for larger radial bins, due to more pairs coming close to the survey boundaries.  $\Phi$  is hence a useful function, since it allows us to simply assess the impact of the survey window on the pair counts at different radial separations and angles, and effectively ‘convert’ between windowed and ideal surveys.

We proceed to insert this into the Legendre-binned 2PCF estimator;

$$\hat{\xi}_\ell^a = \frac{2\ell + 1}{V(nw)^2 v_a} \int_0^1 d\mu L_\ell(\mu) \sum_c \Theta^c(\mu) \Phi(r_a, \mu) \frac{NN_c^a}{\delta\mu} \quad (3.10)$$

converting  $NN^a(\mu)$  to its binned form via Eq. 3.6 and denoting the shell volume as  $v_a = \frac{4\pi}{3} \left( r_{a,\max}^3 - r_{a,\min}^3 \right)$ . The integral can be converted to an additional sum over  $\mu$  bins of (arbitrarily small) width  $\delta\mu$  with centers at  $\mu_n$ ;

$$\hat{\xi}_\ell^a = \frac{2\ell + 1}{V(nw)^2 v_a} \sum_n \delta\mu L_\ell(\mu_n) \sum_c \Theta^c(\mu_n) \Phi(r_a, \mu_n) \frac{NN_c^a}{\delta\mu}. \quad (3.11)$$

We now insert the  $NN_c^a$  estimator (Eq. 2.3) which yields

$$\hat{\xi}_\ell^a = \frac{2\ell + 1}{V(nw)^2 v_a} \sum_n \sum_c \sum_{i \neq j} \Theta^c(\mu_n) \Theta^c(\mu_{ij}) \Theta^a(r_{ij}) L_\ell(\mu_n) \Phi(r_a, \mu_n) n_i n_j w_i w_j \delta_i \delta_j. \quad (3.12)$$

Taking the limit  $\delta\mu \rightarrow 0$ , the binning functions tend to Dirac delta functions which allows us to identify  $\mu_n = \mu_{ij}$ , giving the simplified Legendre-binned 2PCF estimator;

$$\hat{\xi}_\ell^a = \frac{2\ell + 1}{V(nw)^2 v_a} \sum_{i \neq j} n_i n_j w_i w_j \Theta^a(r_{ij}) \Phi(r_a, \mu_{ij}) L_\ell(\mu_{ij}) \delta_i \delta_j \quad (3.13)$$

(valid for even  $\ell$ ). Notably, the survey correction factor  $\Phi$  depends on the radial bin center  $r_a$  rather than the radial separation of each pair of points,  $r_{ij}$ , since it arises from the  $RR^a(\mu)$  pair counts. Although we have only integrated over  $\mu$  here, this formalism can simply be extended to compute similar estimators for  $r$ -integrated statistics, such as the Baryon Acoustic Oscillation (BAO)  $\omega_\ell$  statistic introduced in Xu et al. (2010).

### 3.2 2PCF Covariance Matrix

Using the Legendre-moment 2PCF estimator above (Eq. 3.13), we may define the associated covariance matrix in radial bins  $a, b$  and Legendre indices  $p, q$  in the standard fashion;

$$\text{cov}(\hat{\xi}_p^a, \hat{\xi}_q^b) \equiv C_{pq}^{ab} = \langle \hat{\xi}_p^a \hat{\xi}_q^b \rangle - \langle \hat{\xi}_p^a \rangle \langle \hat{\xi}_q^b \rangle. \quad (3.14)$$

Using the Legendre polynomial expansions (Eq. 3.2) this can be related to the covariance in angular bins  $m, n$  (i.e. Eq. 2.9) via

$$C_{pq}^{ab} \approx (2p + 1)(2q + 1) \int_0^1 d\mu \int_0^1 d\mu' L_p(\mu) L_q(\mu') \sum_{m,n} \Theta^m(\mu) \Theta^n(\mu') (\delta\mu)^{-2} C_{mn}^{ab} \quad (3.15)$$

<sup>2</sup> [corrfunc.readthedocs.io](https://github.com/legosoft/corrfunc.readthedocs.io)

which becomes exact in the limit of infinitely small  $\mu$  bins. As before, we opt to compute this directly, rather than from the angularly binned matrices. Inserting the 2PCF estimators (Eq. 3.13) into Eq. 3.14, we obtain the estimator

$$\begin{aligned} \hat{C}_{pq}^{ab} &= \frac{(2p+1)(2q+1)}{(V(nw)^2)^2 v_a v_b} \sum_{i \neq j} \sum_{k \neq l} n_i n_j n_k n_l w_i w_j w_k w_l \Theta^a(r_{ij}) \Theta^b(r_{kl}) \\ &\times \Phi(r_a, \mu_{ij}) \Phi(r_b, \mu_{kl}) L_p(\mu_{ij}) L_q(\mu_{kl}) \left[ \langle \delta_i \delta_j \delta_k \delta_l \rangle - \langle \delta_i \delta_j \rangle \langle \delta_k \delta_l \rangle \right]. \end{aligned} \quad (3.16)$$

The expansion of the above summation into 2-, 3- and 4-point terms and the application of Wick's theorem is performed exactly as for the  $(r, \mu)$  binned 2PCF covariance (Eqs. 2.6-2.8), which gives the final form

$$C_{pq}^{ab} = {}^4 C_{pq}^{ab} + \alpha \times {}^3 C_{pq}^{ab} + \alpha^2 \times {}^2 C_{pq}^{ab} \quad (3.17)$$

with the definitions

$$\begin{aligned} {}^4 C_{pq}^{ab} &= \frac{(2p+1)(2q+1)}{(V(nw)^2)^2 v_a v_b} \sum_{i \neq j \neq k \neq l} n_i n_j n_k n_l w_i w_j w_k w_l \Theta^a(r_{ij}) \Theta^b(r_{kl}) \\ &\times \Phi(r_a, \mu_{ij}) \Phi(r_b, \mu_{kl}) L_p(\mu_{ij}) L_q(\mu_{kl}) \left[ \xi_{ijkl}^{(4)} + 2\xi_{ik} \xi_{jl} \right] \\ {}^3 C_{pq}^{ab} &= 4 \times \frac{(2p+1)(2q+1)}{(V(nw)^2)^2 v_a v_b} \sum_{i \neq j \neq k} n_i n_j n_k w_i (w_j)^2 w_k \Theta^a(r_{ij}) \Theta^b(r_{jk}) \\ &\times \Phi(r_a, \mu_{ij}) \Phi(r_b, \mu_{jk}) L_p(\mu_{ij}) L_q(\mu_{jk}) \left[ \xi_{ijk} + \xi_{ik} \right] \\ {}^2 C_{pq}^{ab} &= 2\delta_{ab} \times \frac{(2p+1)(2q+1)}{(V(nw)^2)^2 v_a^2} \sum_{i \neq j} n_i n_j (w_i w_j)^2 \Theta^a(r_{ij}) \\ &\times (\Phi(r_a, \mu_{ij}))^2 L_p(\mu_{ij}) L_q(\mu_{ij}) \left[ 1 + \xi_{ij} \right]. \end{aligned} \quad (3.18)$$

As before, these may be transformed into integrals by replacing the summations with integrals and promoting variables to be functions of position. Notably the 2-point function is no-longer diagonal, with off-diagonal elements arising for  $m \neq n$ , due to the Legendre binning.

Practically, the integrals in Eqs. 3.18 may be computed using a similar algorithm to the  $(r, \mu)$ -binning algorithm described in Philcox et al. (2019). As before, sets of four particles can be drawn according to some importance sampling scheme chosen to give efficient integral sampling. Instead of adding the integral contributions of these particles (in some radial bins  $a, b$ ) to a single set of  $\mu$  bins, we may compute contributions to *all*  $(p, q)$ -bins simultaneously, by evaluating the relevant Legendre polynomials. This, coupled with the fact that less Legendre bins are usually required than  $\mu$ -bins, will significantly boost computational speed, sampling  $N_c^2$  more bins for the same number of quads drawn, with little additional computation required. It is important to note that this formalism does not simply extend to the jackknife covariance matrices discussed in O'Connell & Eisenstein (2019) and Philcox et al. (2019). Since these depend on the 2PCFs computed using specific jackknife regions, we would need to introduce survey-correction functions for each individual jackknife as well as each radial bin, greatly increasing the complexity. We note however that the principal use of the jackknife matrices is in determining the shot-noise rescaling parameter  $\alpha$ , which is the same for Legendre-binned and  $\mu$ -binned full covariance matrices. We may thus use  $\mu$ -binned jackknife matrices to constrain  $\alpha$ , which can then be used to compute full Legendre-binned covariances.

### 3.3 Multi-Field 2PCF Covariances

We should additionally consider the Legendre-binned 2PCF covariance matrix arising from two different fields (cf. Philcox et al. 2019, Sec. 6). We first require an approximation for the  $RR$  pair counts between the two fields, labelled  $X$  and  $Y$ . By analogy with the above, the  $R^X R^Y$  integral in radial bin  $a$  and angular bin  $c$  is given by

$$\left( R^X R^Y \right)_c^a = \int d^3 \mathbf{r}_i d^3 \mathbf{r}_j n^X(\mathbf{r}_i) n^Y(\mathbf{r}_j) w^X(\mathbf{r}_i) w^Y(\mathbf{r}_j) \Theta^a(|\mathbf{r}_i - \mathbf{r}_j|) \Theta^c(\mu_{(\mathbf{r}_i - \mathbf{r}_j)}) \quad (3.19)$$

where the superscripts indicate what field the quantity belongs to. As before, we use infinite uniform survey assumptions and a correction factor to yield the continuous random count form

$$\left( R^X R^Y \right)^\alpha(\mu) \equiv \frac{V^X \overline{n^X n^Y w^X w^Y} v_a}{\Phi^{XY}(r_a, \mu)}. \quad (3.20)$$

Here  $V^X$  is the volume of survey  $X$ , and  $\overline{n^X n^Y w^X w^Y}$  is the mean of  $n^X n^Y w^X w^Y$  across the survey. Notably, this appears asymmetric with respect to  $X \leftrightarrow Y$  interchanges, due to presence of only a single factor of volume. The differing volumes of the two surveys are encapsulated by the correction factor  $\Phi^{XY}$  and we here note that  $\Phi^{XY}/V^X = \Phi^{YX}/V^Y$ , restoring the field-interchange symmetry of  $R^X R^Y$ . The survey-correction factors  $\Phi^{XY}$  can be found from comparing the  $R^X R^Y$  model to



computed pair counts, e.g. with `corrfunc`. From this, and adopting the Landy-Szalay generalization

$$\left(\xi^{XY}\right)^a(\mu) = \frac{\left(N^X N^Y\right)^a(\mu)}{\left(R^X R^Y\right)^a(\mu)} \quad (3.21)$$

where  $N^T \equiv D^T - R^T$  for  $T \in \{X, Y\}$ , the Legendre-binned 2PCF estimator becomes

$$\left(\xi^{XY}\right)_\ell^a = \frac{2\ell + 1}{V^X \overline{n^X n^Y} \overline{w^X w^Y} v_a} \sum_{i \neq j} n_i^X n_j^Y w_i^X w_j^Y \Theta^a(r_{ij}) \Phi^{XY}(r_a, \mu_{ij}) L_\ell(\mu_{ij}) \delta_i^X \delta_j^Y \quad (3.22)$$

where  $\delta^X$  and  $\delta^Y$  are the overdensities in fields  $X$  and  $Y$ . The full Legendre-binned covariance matrix follows similarly from this, taking the form

$$\begin{aligned} \left(C^{XY, ZW}\right)_{pq}^{ab} &= \left({}^4 C^{XY, ZW}\right)_{pq}^{ab} + \frac{\alpha^X}{4} \left[\delta^{XW} \left({}^3 C^{X, YZ}\right)_{pq}^{ab} + \delta^{XZ} \left({}^3 C^{X, YW}\right)_{pq}^{ab}\right] + \frac{\alpha^Y}{4} \left[\delta^{YW} \left({}^3 C^{Y, XZ}\right)_{pq}^{ab} + \delta^{YZ} \left({}^3 C^{Y, XW}\right)_{pq}^{ab}\right] \\ &+ \frac{\alpha^X \alpha^Y}{2} \left(\delta^{XW} \delta^{YZ} + \delta^{XZ} \delta^{YW}\right) \left({}^2 C^{XY}\right)_{pq}^{ab}. \end{aligned}$$

where  $\alpha^X$  and  $\alpha^{XY}$  are shot-noise rescaling parameters for fields  $X$  and  $Y$  and  $\delta^{XY}$  etc. are Kronecker deltas. The 2-, 3- and 4-point components are defined by

$$\begin{aligned} \left({}^4 C^{XY, ZW}\right)_{pq}^{ab} &= \frac{(2p+1)(2q+1)}{V^X V^Z \overline{n^X n^Y} \overline{w^X w^Y} \overline{n^Z n^W} \overline{w^Z w^W} v_a v_b} \sum_{i \neq j \neq k \neq l} n_i^X n_j^Y n_k^Z n_l^W w_i^X w_j^Y w_k^Z w_l^W \Theta^a(r_{ij}) \Theta^b(r_{kl}) \\ &\times \Phi^{XY}(r_a, \mu_{ij}) \Phi^{ZW}(r_b, \mu_{kl}) L_p(\mu_{ij}) L_q(\mu_{kl}) \left[\xi_{ijkl}^{(4), XYZW} + \xi_{ik}^{XZ} \xi_{jl}^{YW} + \xi_{il}^{XW} \xi_{jk}^{YZ}\right] \\ \left({}^3 C^{Y, XZ}\right)_{pq}^{ab} &= 4 \times \frac{(2p+1)(2q+1)}{V^X V^Z \overline{n^X n^Y} \overline{w^X w^Y} \overline{n^Y n^Z} \overline{w^Y w^Z} v_a v_b} \sum_{i \neq j \neq k} n_i^X n_j^Y n_k^Z w_i^X \left(w_j^Y\right)^2 w_k^Z \Theta^a(r_{ij}) \Theta^b(r_{jk}) \\ &\times \Phi^{XY}(r_a, \mu_{ij}) \Phi^{ZY}(r_b, \mu_{jk}) L_p(\mu_{ij}) L_q(\mu_{jk}) \left[\xi_{ijk}^{XYZ} + \xi_{ik}^{XZ}\right] \\ \left({}^2 C^{XY}\right)_{pq}^{ab} &= 2\delta_{ab} \times \frac{(2p+1)(2q+1)}{\left(V^X \overline{n^X n^Y} \overline{w^X w^Y} v_a\right)^2} \sum_{i \neq j} n_i^X n_j^Y \left(w_i^X w_j^Y\right)^2 \Theta^a(r_{ij}) \\ &\times \left(\Phi^{XY}(r_a, \mu_{kl})\right)^2 L_p(\mu_{ij}) L_q(\mu_{ij}) \left[1 + \xi_{ij}^{XY}\right]. \end{aligned} \quad (3.24)$$

These expressions reduce to the single-field 2PCF covariances (Eqs. 3.18) in the limit  $X = Y = Z = W$ , and may be computed in the same manner as the  $(r, \mu)$ -space multi-field 2PCF covariance integrals, described in Philcox et al. (2019, Sec. 6). Notably the inclusion of multiple fields gives two distinct Gaussian 4-point terms, which involve  $\xi_{ik}^{XZ} \xi_{jl}^{YW}$  and  $\xi_{il}^{XW} \xi_{jk}^{YZ}$ , unlike the single  $2\xi_{ik} \xi_{jl}$  term present previously. As in previous work, for a two-field scenario (denoted  $S$  and  $T$ ), if we compute the  $C^{ST, TS}$  term (and its symmetries) as the average of  $C^{ST, TS}$  and  $C^{ST, ST}$ , we can assume this symmetry to hold, greatly expediting computation.

### 3.4 Comparison with Mock Legendre Covariances

The integrals of Sec. 3.2 and 3.3 may be computed with small modification to the algorithm described in Philcox et al. (2019), and have been implemented into the `RascalC` pipeline for both one and two sets of tracer particles. To assess whether our algorithm and covariance matrix formalism is producing correct results, we use the `RascalC` code to compute a 2PCF covariance matrix in Legendre polynomial bins, which may be compared to a sample covariance derived from a set of Quick Particle Mesh (QPM; White et al. 2014) mocks created for the CMASS-N survey from Data Release 12 of the Baryon Oscillation Spectroscopic Survey (BOSS; Alam et al. 2015, 2017), part of the Sloan Digital Sky Survey III (SDSS-III; Eisenstein et al. 2011). In this test, the input 2PCF (used in the covariance integrals) is computed from the mean of 1000 finely-binned QPM (White et al. 2014) mock galaxy correlation functions. All even multipoles up to  $\ell = 6$  are used, with a covariance matrix radial binning scheme of  $r \in [40, 180]h^{-1}$  Mpc and  $\Delta r = 4h^{-1}$  Mpc, giving a total of 35 radial bins and four Legendre bins. Here, we use a random particle file provided by BOSS for clustering analyses, which uses  $N_{\text{rand}} = 10N_{\text{gal}} = 6420510$  particles, and we adopt FKP (Feldman et al. 1994) weights. Before running the main code, `RR` pair counts are computed using `corrfunc` (Sinha & Garrison 2017) for 35 radial bins (as above) and 100 angular bins which are fit to the boundless infinite survey model to determine the correction function  $\Phi$  for each radial bin as a function of  $\mu$  (cf. Eq. 3.9), using  $V(nw)^2 = 7.07h^3 \text{Mpc}^{-3}$ . In radial bin  $a$ ,  $\Phi$  is parametrized as a polynomial function;

$$\Phi^a(\mu) = \begin{cases} \beta_0^a + \beta_1^a \mu + \beta_2^a \mu^2 & \text{if } 0 \geq \mu \geq 0.75 \\ \gamma_0^a + \gamma_1^a \mu + \gamma_2^a \mu^2 + \gamma_3^a \mu^3 & \text{else,} \end{cases} \quad (3.25)$$

with three components set by ensuring continuity and smoothness up to  $d^2\Phi^a/d\mu^2$  at  $\mu = 0.75$ . The piecewise function is adopted to account for the different behaviour of  $\mu$  near unity, due to RSD effects. The free components  $\{\beta^a\}, \{\gamma^a\}$  are here fit using `scipy`. Following this, the covariance integrals are estimated using a total of  $8 \times 10^{12}$  quads of particles, taking  $\sim 200$  CPU-hours to compute. As in previous works, non-Gaussianity is encapsulated via the inclusion of the shot-noise rescaling parameter,  $\alpha$ , calibrated using jackknife matrices. As previously mentioned, the above conversions of  $(r, \mu)$  binning to Legendre binning do not apply for jackknife matrices, thus we adopt the value  $\alpha = 1.032$  for this mock, as found in [Philcox et al. \(2019\)](#).

For the sample covariance matrix, we estimate the Legendre-moments of the anisotropic 2PCF,  $\hat{\xi}_\ell(r)$ , for 99 individual QPM mocks, using pair counts computed for  $\Delta\mu = 1/120$  and  $\Delta r = 4h^{-1}$  Mpc. Given a radial bin  $a$  and a set of  $\mu$ -bins spanning  $[0, 1]$  with centers at  $\{\mu_c\}$ , we estimate the Legendre-binned 2PCF in mock  $n$  as

$$\hat{\xi}_\ell^{(n),a} \approx (2\ell + 1)\Delta\mu \sum_c \hat{\xi}_c^{(n),a} L_\ell(\mu_c), \quad (3.26)$$

which becomes exact in the limit  $\Delta\mu \rightarrow 0$  (and is simply the discretized form of Eq. 3.3). The sample covariance matrix in radial bins  $a, b$  and Legendre moments  $p, q$  is computed as

$$\hat{C}_{pq}^{ab} = \text{cov}(\hat{\xi}_p^a, \hat{\xi}_q^b) = \frac{1}{N_{\text{mocks}} - 1} \sum_{n=1}^{N_{\text{mocks}}} \left[ \left( \hat{\xi}_p^{(n),a} - \bar{\xi}_p^a \right) \left( \hat{\xi}_q^{(n),b} - \bar{\xi}_q^b \right) \right] \quad (3.27)$$

where  $\bar{\xi}$  indicates the mean over all 99 mocks. Despite the large number of  $\mu$ -bins used here, we do not necessarily expect perfect agreement between our code and the QPM mocks here as the 2PCF greatly changes as  $\mu \rightarrow 1$ , leading to non-negligible errors due to the finite binning.

Before comparing theory and mock observations, we first we consider the structure of the covariance matrix estimate. In Fig. 2, the correlation matrix  $R_{pq}^{ab}$  is displayed for all even Legendre moment pairs  $\{p, q\}$  up to the sixth moment, defining

$$R_{pq}^{ab} = C_{pq}^{ab} / \sqrt{C_{pp}^{aa} C_{qq}^{bb}}. \quad (3.28)$$

Notably, we observe strong positive correlations between bins with  $p = q$ , which are largest for  $r_a \approx r_b$ . These grow weaker both as  $|r_a - r_b|$  and  $|p - q|$  increase, with the  $p = q + 2$  submatrices displaying weakly positive correlations for  $r_a < r_b$  and negative else. Analysis of the  $C_{ab}^{pq}$  matrix itself shows small covariances for  $\{p, q\} = \{0, 0\}$ , which grow greater for higher  $\ell$ , reflecting the increased difficulty in observing higher multipoles.

For comparison of theory and simulation, we require precision matrices, which, in the limit of zero noise (or  $N_{\text{mocks}} \rightarrow \infty$ ), are defined simply as covariance matrix inverses. As shown in [Wishart \(1928\)](#) and [Hartlap et al. \(2007\)](#), for finite  $N_{\text{mocks}}$ , we must instead use the (compressed) sample precision matrix definition

$$\begin{aligned} \Psi_{\text{sample}} &= (1 - D)\hat{\mathbf{C}}_{\text{sample}}^{-1} \\ D &= \frac{N_{\text{bins}} + 1}{N_{\text{mocks}} - 1} \end{aligned} \quad (3.29)$$

to avoid a non-negligible bias. For the theoretical covariance matrix, which is not expected to obey Wishart statistics, we take a different approach, made possible by obtaining a set  $\{\hat{\mathbf{C}}_i\}$  of  $N_{\text{samples}}$  independent theoretical covariance matrix estimates. The bias-corrected precision is then defined as;

$$\begin{aligned} \Psi_{\text{theory}} &= (\mathbb{I} - \tilde{\mathbf{D}})\hat{\mathbf{C}}^{-1} \\ \tilde{\mathbf{D}} &= \frac{N_{\text{samples}} - 1}{N_{\text{samples}}} \left[ -\mathbb{I} + \frac{1}{N_{\text{samples}}} \sum_i \hat{\mathbf{C}}_{[i]}^{-1} \hat{\mathbf{C}}_i \right] \end{aligned} \quad (3.30)$$

([O'Connell & Eisenstein 2019](#)), where  $\hat{\mathbf{C}}_{[i]}$  is the mean of the covariance matrix estimates, excluding  $\hat{\mathbf{C}}_i$ . Since the `RascalC` algorithm is fully stochastic, we can easily compute independent matrix estimates by running the algorithm multiple times. The  $\tilde{\mathbf{D}}$  matrix may also be used to assess the matrix convergence via the ‘effective number of mocks’, defined by

$$N_{\text{eff}} = \frac{N_{\text{bins}} + 1}{|\tilde{\mathbf{D}}|^{1/N_{\text{bins}}}} + 1$$

(cf. [Philcox et al. 2019](#), Sec. 3.4). Here, using  $N_{\text{samples}} = 20$ , we obtain  $N_{\text{eff}} = 6 \times 10^6$ , implying that our matrix has the same noise level as one constructed from six million mocks, greatly subdominant to the Wishart noise in the QPM covariance created from 99 mocks. We caution that  $N_{\text{eff}}$  purely parametrizes the noise level from the numerical sampling. There is an additional (non-stochastic) source of error from the approximations made in our theoretical model (i.e. that the higher-point correlation functions can be modelled by increased shot-noise), which is more difficult to estimate. Here we probe this by comparing our estimates to those from mocks, though it is not certain how well the non-Gaussianity of the mocks themselves represents our Universe.

To assess the systematic difference between the Legendre matrix estimates, we use the ‘discriminant’ matrix

$$\mathbf{P} = \sqrt{\Psi_{\text{RascalC}}}^T \mathbf{C}_{\text{QPM}} \sqrt{\Psi_{\text{RascalC}}} - \mathbb{I} \quad (3.31)$$

(suppressing matrix components for clarity), where  $\Psi_{\text{RascalC}}$  is the theoretical precision matrix (from Eq. 3.30),  $\mathbf{C}_{\text{QPM}}$  is the



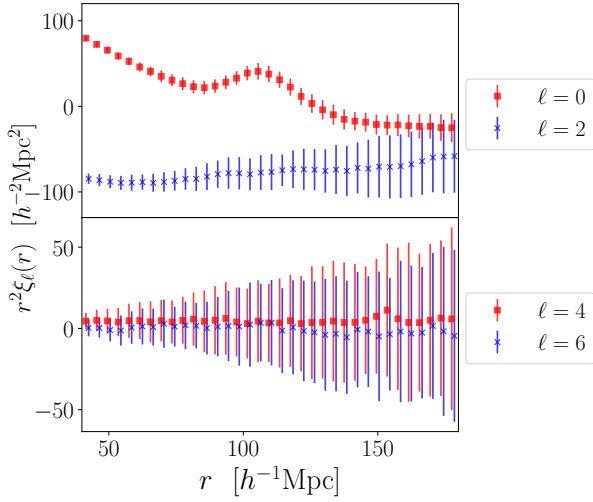


**Figure 1.** Measured two-point correlation function (2PCF) multipoles from 99 Quick Particle Mesh (QPM; White et al. 2014) BOSS DR12 mocks, computed with the `corrfunc` code (Sinha & Garrison 2017). In each mock, we measure the 2PCF from  $\sim 6 \times 10^5$  using the Landy & Szalay (1993) estimator in a total of 35 radial bins and 100 angular bins, before conversion into Legendre polynomial space via Eq. 3.3. The displayed errors (computed as the standard deviation of the 99 2PCF measurements) represent the precision achievable from a single galaxy survey, and a small lateral displacement is added to the  $\ell = 2$  and 6 data-sets for visibility. We note highly significant monopole and quadrupole detections but little power in the higher multipoles.

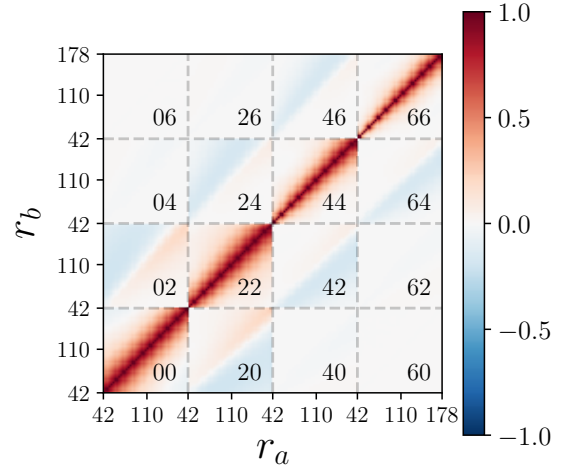


**Figure 2.** Theoretical correlation matrix (Eq. 3.28) for the anisotropic 2PCF estimates displayed in Fig. 1. Individual pixels represent the correlations at a pair of radial bins  $\{a, b\}$ , and we display results for 16 pairs of Legendre multipoles,  $\{p, q\}$ , with each pair in a separate sub-matrix, as indicated by the text. This matrix is computed with the `RascalC` code in  $\sim 200$  CPU-hours, sampling covariance matrix integrals using a random particle catalog appropriate for the BOSS DR12 CMASS-N geometry (Alam et al. 2017). The estimator uses the mean correlation function estimated from 1000 QPM mock galaxy surveys, and non-Gaussianity is incorporated by way of a shot-noise rescaling parameter  $\alpha = 1.032$ , as found by Philcox et al. (2019). As described in the main text, the theoretical matrix has a noise level from numerical errors equivalent to that of  $\sim 6 \times 10^6$  mocks, though the error from systematics may be significantly larger. We note strongest correlations for identical multipoles which are weaker as  $|p - q|$  increases.

QPM covariance,  $\mathbb{I}$  is the identity matrix and the square-root indicates the lower Cholesky decomposition. Note that we invert only the theoretical matrix here, since  $N_{\text{mocks}}$  is low, leading to a severely biased sample precision matrix. The discriminant matrix is plotted in Fig. 4, and any systematic deviations from unity indicate differences between the approaches. In this instance, we do not observe any obvious deviations between the matrices given the level of noise. Indeed, the matrix is found to have a mean and root-mean-square value of 0.05% and 13% respectively, which matches the expected deviations of  $N_{\text{DoF}}/\sqrt{N_{\text{mocks}}} \sim 14\%$  from noise alone, for  $N_{\text{DoF}} = 140$  degrees of freedom. At higher  $\ell$ , there are slightly increased deviations along the main diagonal, which we attribute to the increasing error arising from the  $\mu$ -binning at larger Legendre moment. The clear strong agreement between the matrices indicates that our  $RR$  window-correction function approximation has been successful and that our algorithm works as expected.

## 4 ESTIMATING THE THREE POINT CORRELATION FUNCTION

### 4.1 3PCF Estimator in Angular Bins

The above formalism may be generalized to the isotropic three-point correlation function (3PCF),  $\zeta$ . The standard Szapudi-Szalay estimator gives

$$\zeta(r_1, r_2, \chi) = \frac{NNN(r_1, r_2, \chi)}{RRR(r_1, r_2, \chi)} \quad (4.1)$$

(Szapudi & Szalay 1998) for  $N = D - R$  as before, parametrizing the 3PCF via the lengths of two sides ( $r_1$  and  $r_2$ ) and the cosine of the angle between them,  $\chi$ .<sup>3</sup> Given radial bins  $a, b$  and  $\chi$ -bin  $c$ , the binned triple counts are defined in small cells

<sup>3</sup> In this paper  $\mu$  refers to cosines of angles between a pair of particles and the LoS and  $\chi$  refers to triangle internal angles. Unlike for  $\mu$ , the sign of  $\chi$  is important here, thus we do not take the modulus.

(each of which containing at most one particle) as

$$\begin{aligned} NNN_c^{ab} &= \sum_{i \neq j \neq k} n_i n_j n_k w_i w_j w_k \delta_i \delta_j \delta_k \tilde{\Theta}_{ijk}^{ab,c} \\ RRR_c^{ab} &= \sum_{i \neq j \neq k} n_i n_j n_k w_i w_j w_k \tilde{\Theta}_{ijk}^{ab,c}. \end{aligned} \quad (4.2)$$

analogously to the  $RR$  and  $NN$  counts (Eq. 2.3). The binning function  $\tilde{\Theta}_{ijk}^{ab,c}$  selects triangles of the correct orientation via

$$\tilde{\Theta}_{ijk}^{ab,c} = \begin{cases} 1 & \text{if } |\mathbf{r}_{YX}| \text{ is in bin } a \text{ and } |\mathbf{r}_{ZX}| \text{ is in bin } b \text{ and } \chi_{YZ} = \frac{(\mathbf{r}_{YX}) \cdot (\mathbf{r}_{ZX})}{|\mathbf{r}_{YX}| |\mathbf{r}_{ZX}|} \text{ is in bin } c \\ 0 & \text{else.} \end{cases} \quad (4.3)$$

denoting  $\mathbf{r}_{XY} = \mathbf{r}_X - \mathbf{r}_Y$  etc., where  $X, Y, Z$  are some permutation of  $\{i, j, k\}$ . Importantly, this is symmetric under any permutation of the indices  $i, j, k$ , as are the summands in Eqs. 4.2. We may equivalently write this as a product of univariate binning functions,

$$\tilde{\Theta}_{ijk}^{ab,c} = \left[ \Theta^a(r_{ij}) \Theta^b(r_{ik}) \Theta^c(\chi_{jk}) + 5 \text{ perms.} \right], \quad (4.4)$$

summing over the six distinct triangle configurations, with  $r = |\mathbf{r}|$  and  $\chi_{jk}$  being the cosine of the angle between the vectors  $\mathbf{r}_j - \mathbf{r}_i$  and  $\mathbf{r}_k - \mathbf{r}_i$ . The full 3PCF estimator thus becomes

$$\hat{\zeta}_c^{ab} = \frac{1}{RRR_c^{ab}} \sum_{i \neq j \neq k} n_i n_j n_k w_i w_j w_k \delta_i \delta_j \delta_k \tilde{\Theta}_{ijk}^{ab,c}. \quad (4.5)$$

## 4.2 Legendre Moment 3PCF Estimator

The Legendre moments of the 3PCF may be computed in an analogous fashion to the 2PCF (following Szapudi 2004; Slepian & Eisenstein 2015b), by way of a survey-correction function (as in Sec. 3.1). We first consider an alternative form for the  $RRR_c^{ab}$  triple count in radial bins  $(a, b)$  and small angular bin  $\delta\chi$  (which is later shrunk to infinitesimal width). Due to the relabelling symmetry of Eq. 4.2 under permutations of  $\{i, j, k\}$ , all six  $RRR$  terms arising from the different triangle configurations (Eq. 4.4) are identical, which gives

$$RRR_c^{ab} = 6 \sum_{i \neq j \neq k} n_i n_j n_k w_i w_j w_k \Theta^a(r_{ij}) \Theta^b(r_{ik}) \Theta^c(\chi_{jk}) \quad (4.6)$$

(the  $NNN$  estimator exhibits similar behavior). Converting the summation into an integral over the survey gives

$$RRR_c^{ab} = 6 \int d^3\mathbf{x} d^3\mathbf{y} d^3\mathbf{z} n(\mathbf{x}) n(\mathbf{y}) n(\mathbf{z}) w(\mathbf{x}) w(\mathbf{y}) w(\mathbf{z}) \Theta^a(|\mathbf{y} - \mathbf{x}|) \Theta^b(|\mathbf{z} - \mathbf{x}|) \Theta^c(\chi_{(\mathbf{z}-\mathbf{y})}) \quad (4.7)$$

where  $\chi_{(\mathbf{z}-\mathbf{y})}$  indicates the angle between the vectors  $\mathbf{z} - \mathbf{x}$  and  $\mathbf{y} - \mathbf{x}$ . For an infinite uniform survey we can extract the factors of  $n$  and  $w$  and transform variables to  $\mathbf{t} = \mathbf{y} - \mathbf{x}$  and  $\mathbf{u} = \mathbf{z} - \mathbf{x}$ ;

$$RRR_c^{ab} = 6(nw)^3 \left[ \int d^3\mathbf{x} \right] \left[ \int d^3\mathbf{t} d^3\mathbf{u} \Theta^a(|\mathbf{t}|) \Theta^b(|\mathbf{u}|) \Theta^c(\chi_{(\mathbf{t}-\mathbf{u})}) \right]. \quad (4.8)$$

The integral over  $\mathbf{x}$  gives a factor of the survey volume  $V$  and we may additionally rotate the  $\mathbf{u}$  to  $\tilde{\mathbf{u}}$  coordinate such that  $\chi_{\tilde{\mathbf{u}}} = 0$  without affecting the radial parts, giving

$$\begin{aligned} RRR_c^{ab} &\approx 6V(nw)^3 \int d^3\mathbf{t} d^3\tilde{\mathbf{u}} \Theta^a(|\mathbf{t}|) \Theta^b(|\tilde{\mathbf{u}}|) \Theta^c(\chi_t) \\ &= 6V(nw)^3 \times 4\pi \int d\tilde{u} \Theta^a(\tilde{u}) \times 2\pi \int t^2 dt \Theta^b(t) \int d\chi_t \Theta^c(\chi_t) \\ &\approx 3V(nw)^3 \times v_a \times v_b \delta\chi \end{aligned} \quad (4.9)$$

In the final line, we have performed the integrals over the binning function (without restricting to positive  $\chi$ , unlike for the Legendre-binned 2PCF), recalling  $v_a = 4\pi (r_{a,\max}^3 - r_{a,\min}^3) / 3$  (or  $4\pi r_a^2 \Delta r$  in the thin-bin limit). As for the  $RR$  pair counts, we introduce a survey correction factor  $\Phi(r_a, r_b, \chi)$  to make this expression exact for non-uniform and aperiodic surveys (itself now depending on two radial bins and an angle);

$$RRR^{ab}(\chi) \equiv \frac{3V(nw)^3 v_a v_b}{\Phi(r_a, r_b, \chi)} \quad (4.10)$$

also converting to a continuous function in  $\chi$ , with  $\overline{(nw)^3}$  being the survey-averaged value of  $(nw)^3$ . Notably  $\Phi(r_a, r_b, \chi)$  is symmetric under  $a \leftrightarrow b$  interchange.

The Legendre moments of the 3PCF are defined as

$$\hat{\zeta}_\ell^{ab} = \frac{2\ell + 1}{2} \int_{-1}^1 d\chi \frac{NNN^{ab}(\chi)}{RRR^{ab}(\chi)} L_\ell(\chi) \quad (4.11)$$

(cf. Eq. 3.2) where  $L_\ell(\chi)$  is the Legendre polynomial of order  $\ell$ . Note that we must include both odd and even  $\ell$  here (unlike for the 2PCF) due to the lack of  $\chi \rightarrow -\chi$  symmetry. As before, we may write

$$NNN^{ab}(\chi) = \sum_c NNN_c^{ab} \Theta^c(\chi) / \delta\chi \quad (4.12)$$

for infinitesimal bin-size  $\delta\chi$ , which, combined with the continuous random triple count (Eq. 4.10), gives

$$\hat{\xi}_\ell^{ab} = \frac{2\ell + 1}{6V(nw)^3 v_a v_b} \frac{1}{\delta\chi} \int_0^1 d\chi \sum_c \Theta^c(\chi) NNN_c^{ab} L_\ell(\chi) \Phi(r_a, r_b, \chi). \quad (4.13)$$

Including the full estimator for  $NNN$  (Eq. 4.2) using an asymmetric binning function (cf. Eq. 4.6) gives

$$\zeta_\ell^{ab} = \frac{2\ell + 1}{6V(nw)^3 v_a v_b} \frac{1}{\delta\chi} \int_0^1 d\chi \sum_c \Theta^c(\chi) L_\ell(\chi) \Phi(r_a, r_b, \chi) \times 6 \sum_{i \neq j \neq k} \Theta^c(\chi_{jk}) \Theta^a(r_{ij}) \Theta^b(r_{ik}) n_i n_j n_k w_i w_j w_k \delta_i \delta_j \delta_k. \quad (4.14)$$

As before, we integrate over  $\chi$  in the  $\delta\chi \rightarrow 0$  limit, noting that this requires  $\chi = \chi_{jk}$ . Returning to a form symmetric under  $\{i, j, k\}$  permutations, we obtain

$$\xi_\ell^{ab} = \frac{2\ell + 1}{6V(nw)^3 v_a v_b} \sum_{i \neq j \neq k} n_i n_j n_k w_i w_j w_k \delta_i \delta_j \delta_k \tilde{K}_{ijk}^{ab, \ell} \quad (4.15)$$

for symmetrized kernel function (cf. Eq. 4.3)

$$K_{ijk}^{ab, \ell} = \left[ \Theta^a(r_{ij}) \Theta^b(r_{ik}) L_\ell(\chi_{jk}) \Phi(r_a, r_b, \chi_{jk}) + 5 \text{ perms.} \right]. \quad (4.16)$$

This is simply equal to  $2L_\ell(\chi_{ab})\Phi(r_a, r_b, \chi_{ab})$  for a triangle with one side in bin  $a$ , one side in bin  $b$  and opening angle  $\chi_{ab}$ . In practice, given a triplet of particles, we can compute contributions to the 3-point integral for each Legendre multipole in every  $(a, b)$  pair of radial bins that the triplet falls into (with different radial bins arising from different  $\{i, j, k\}$  permutations). A naïve triple count over all particles in a survey using this estimator would count each particle six times; we include this degeneracy to simplify later covariance computations. The form presented above may be naturally extended to the anisotropic 3PCF estimator using spherical harmonic functions rather than Legendre polynomials in the kernel function, as in Slepian & Eisenstein (2018).

## 5 THREE-POINT CORRELATION FUNCTION COVARIANCE MATRICES

### 5.1 Cross Covariance of the 3PCF and 2PCF

Given the anisotropic 2PCF and 3PCF estimators (Eqs. 3.13 & 4.15) we may construct the cross-covariance between them. We initially work in the Legendre basis, which is more efficient since it requires far fewer angular bins and is faster to compute. For radial bins  $a, b$  ( $c$ ) and Legendre moment  $p$  ( $q$ ) for the 3PCF (2PCF), the cross-covariance is defined as

$$\text{cov}(\hat{\xi}_p^{ab}, \hat{\xi}_q^c) \equiv C_{p,q}^{ab,c} = \langle \hat{\xi}_p^{ab} \hat{\xi}_q^c \rangle - \langle \hat{\xi}_p^{ab} \rangle \langle \hat{\xi}_q^c \rangle. \quad (5.1)$$

Inserting the relevant 2PCF and 3PCF estimators, we obtain

$$C_{p,q}^{ab,c} = \frac{(2p+1)(2q+1)}{6V^2(nw)^3 (nw)^2 v_a v_b v_c} \sum_{i \neq j \neq k} \sum_{l \neq m} n_i n_j n_k n_l n_m w_i w_j w_k w_l w_m \times K_{ijk}^{ab,p} \Theta^c(r_{lm}) L_q(\mu_{lm}) \Phi(r_c, \mu_{lm}) \times [\langle \delta_i \delta_j \delta_k \delta_l \delta_m \delta_n \rangle - \langle \delta_i \delta_j \delta_k \rangle \langle \delta_l \delta_m \delta_n \rangle] \quad (5.2)$$

We may expand this into three-, four- and five-point terms using the result

$$\sum_{i \neq j \neq k \neq l \neq m} X_{ijk} Y_{lm} = \sum_{i \neq j \neq k \neq l \neq m} X_{ijk} Y_{lm} + 6 \sum_{i \neq j \neq k \neq l} X_{ijk} Y_{li} + 6 \sum_{i \neq j \neq k} X_{ijk} Y_{ij} \quad (5.3)$$

where  $X_{ijk}$  and  $Y_{lm}$  are totally symmetric under argument permutations.<sup>4</sup> To proceed we must expand the expectations of the overdensity fields  $\delta$  in the three-, four- and five-point terms. Denoting an  $n$ -point connected correlation function  $\xi_{x_1 \dots x_n}^{(n)}$  by  $(x_1 \dots x_n)$ , we may use Wick's theorem to show

$$\begin{aligned} \langle \delta_i \delta_j \delta_k \delta_l \delta_m \delta_n \rangle - \langle \delta_i \delta_j \delta_k \rangle \langle \delta_l \delta_m \delta_n \rangle &= (ijklm) + [(ij)(klm) + (ik)(jlm) + (jk)(ilm)] \\ &+ [(il)(jkm) + (im)(jkl) + (jl)(ikm) + (jm)(ikl) + (kl)(ijm) + (km)(ijl)] \\ \frac{n_i}{\alpha} \langle \delta_i \delta_j \delta_k \delta_l \delta_i \rangle &= \langle (1 + \delta_i)(\delta_j \delta_k \delta_l) \rangle = (ijkl) + (jkl) + [(ij)(kl) + (ik)(jl) + (il)(jk)] \\ \frac{n_i n_j}{\alpha^2} \langle \delta_i \delta_j \delta_k \delta_i \delta_j \rangle &= \langle (1 + \delta_i)(1 + \delta_j) \delta_k \rangle = (ijk) + (ik) + (jk) \end{aligned} \quad (5.4)$$

<sup>4</sup> This is obtained by noting that there are six ways to contract both one and two indices drawn from sets of two and three equivalent indices.

This has made use of the shot-noise contraction approximation of Eq. 2.7. Further simplifications can be made via the relabelling symmetries of the summands under index permutation, for example, in the five-point term,  $\xi_{ij}\zeta_{klm}$  may be transformed into  $\xi_{ik}\zeta_{jlm}$  by relabelling  $j \leftrightarrow k$ , which does not change the summed quantity. In the expressions above, all quantities in square parentheses are similarly equal when we sum over particles. Inserting these contractions into the covariance matrix estimator (Eq. 5.2) and splitting into three-, four- and five-point terms via Eq. 5.3 gives

$$C_{p,q}^{ab,c} = {}^5C_{p,q}^{ab,c} + \alpha \times {}^4C_{p,q}^{ab,c} + \alpha^2 \times {}^3C_{p,q}^{ab,c} \quad (5.5)$$

using the definitions (presented here as summations but easily convertible into integrals as before)

$$\begin{aligned} {}^5C_{p,q}^{ab,c} &= \frac{(2p+1)(2q+1)}{6V^2(nw)^3(nw)^2v_av_bv_c} \sum_{i \neq j \neq k \neq l \neq m} n_i n_j n_k n_l n_m w_i w_j w_k w_l w_m \times K_{ijk}^{ab,p} \Theta^c(r_{lm}) L_q(\mu_{lm}) \Phi(r_a, \mu_{lm}) \\ &\times \left[ \xi_{ijklm}^{(5)} + 3\xi_{ij}\zeta_{klm} + 6\xi_{il}\zeta_{jkm} \right] \\ {}^4C_{p,q}^{ab,c} &= 6 \times \frac{(2p+1)(2q+1)}{6V(nw)^3(nw)^2v_av_bv_c} \sum_{i \neq j \neq k \neq l} n_i n_j n_k n_l (w_i)^2 w_j w_k w_l \times K_{ijk}^{ab,p} \Theta^c(r_{il}) L_q(\mu_{li}) \Phi(r_c, \mu_{li}) \\ &\times \left[ \xi_{ijkl}^{(4)} + \zeta_{jkl} + 3\xi_{ij}\xi_{kl} \right] \\ {}^3C_{p,q}^{ab,c} &= 6 \times \frac{(2p+1)(2q+1)}{6V^2(nw)^3(nw)^2v_av_bv_c} \sum_{i \neq j \neq k} n_i n_j n_k (w_i w_j)^2 w_k \times K_{ijk}^{ab,p} \Theta^c(r_{ij}) L_q(\mu_{ij}) \Phi(r_c, \mu_{ij}) \\ &\times \left[ \zeta_{ijk} + 2\xi_{ik} \right] \end{aligned} \quad (5.6)$$

with the Gaussian terms marked in blue. Notably, there is no Gaussian contribution to the five-point term here, thus all Gaussian components of this covariance arise from shot-noise contractions. If there exists some model (or function interpolated from data) for the 3PCF, the full covariance may be computed by drawing sets of five particles, and computing their contributions to the relevant bins. Each set of five particles will contribute to up to three pairs of 3PCF radial bins  $a, b$  (due to the three triangle sides), a single 2PCF radial bin  $c$  and all required Legendre moment pairs  $p, q$ . If we are interested in computing only the Gaussian contribution, we need only draw sets of four particles, significantly expediting computation.

If instead we desired this correlation functions directly in  $\mu$ -bins rather than Legendre multipoles (used in clustering wedges e.g. Kazin et al. 2012; Sánchez et al. 2017), we may use a similar expansion as above, with a slightly modified summand. This gives the expression (for internal triangle angle  $\chi$ -bin  $d$  and pairwise LoS  $\mu$ -bin  $e$ )

$$\begin{aligned} \text{cov}(\hat{\zeta}_d^{ab}, \hat{\xi}_e^c) &= {}^5C_{d,e}^{ab,c} + \alpha \times {}^4C_{d,e}^{ab,c} + \alpha^2 \times {}^3C_{d,e}^{ab,c} \quad (5.7) \\ {}^5C_{d,e}^{ab,c} &= \frac{1}{RRR_d^{ab} RR_e^c} \sum_{i \neq j \neq k \neq l \neq m} n_i n_j n_k n_l n_m w_i w_j w_k w_l w_m \tilde{\Theta}_{ijk}^{ab,d} \Theta^c(r_{lm}) \Theta^e(\mu_{lm}) \\ &\times \left[ \xi_{ijklm}^{(5)} + 3\xi_{ij}\zeta_{klm} + 6\xi_{ijl}\xi_{km} \right] \\ {}^4C_{d,e}^{ab,c} &= \frac{6}{RRR_d^{ab} RR_e^c} \sum_{i \neq j \neq k \neq l} n_i n_j n_k n_l (w_i)^2 w_j w_k w_l \tilde{\Theta}_{ijk}^{ab,d} \Theta^c(r_{li}) \Theta^e(\mu_{li}) \\ &\times \left[ \xi_{ijkl}^{(4)} + \zeta_{jkl} + 3\xi_{ij}\xi_{kl} \right] \\ {}^3C_{d,e}^{ab,c} &= \frac{6}{RRR_d^{ab} RR_e^c} \sum_{i \neq j \neq k} n_i n_j n_k (w_i w_j)^2 w_k \tilde{\Theta}_{ijk}^{ab,d} \Theta^c(r_{ij}) \Theta^e(\mu_{ij}) \\ &\times \left[ \zeta_{ijk} + 2\xi_{ik} \right] \end{aligned}$$

which may be computed in a similar fashion to the Legendre-binned function, except that one would add contributions to a single pair of angular bins for a given set of five particles and triangle configuration, rather than all combinations of multipoles.

## 5.2 Auto-covariance of the 3PCF

### 5.2.1 Theoretical Estimators

The auto-covariance of the 3PCF,  $\zeta$ , may be found analogously to the above, involving decomposition into three-, four-, five- and six-point summations (or integrals in the continuous limit). Using  $a, b$  ( $c, d$ ) to denote the radial bins and  $p$  ( $q$ ) the

Legendre multipole of the first (second) isotropic 3PCF, we obtain the expression

$$\begin{aligned} \text{cov} \left( \hat{\xi}_p^{ab}, \hat{\xi}_q^{cd} \right) &\equiv C_{p,q}^{ab,cd} = \langle \hat{\xi}_p^{ab} \hat{\xi}_q^{cd} \rangle - \langle \hat{\xi}_p^{ab} \rangle \langle \hat{\xi}_q^{cd} \rangle \\ &= \frac{(2p+1)(2q+1)}{\left[6V(\overline{nw})^3\right]^2} \sum_{i \neq j \neq k} \sum_{l \neq m \neq n} n_i n_j n_k n_l n_m n_n w_i w_j w_k w_l w_m w_n \times K_{ijk}^{ab,p} K_{lmn}^{cd,q} \\ &\times \left[ \langle \delta_i \delta_j \delta_k \delta_l \delta_m \delta_n \rangle - \langle \delta_i \delta_j \delta_k \rangle \langle \delta_l \delta_m \delta_n \rangle \right] \end{aligned} \quad (5.8)$$

using the 3PCF definition and Legendre kernel function of Eqs. 4.15 & 4.16. Note that the summand is symmetric under any permutation of  $\{i, j, k\}$  or  $\{l, m, n\}$ . As before, this may be expanded with the identity

$$\sum_{i \neq j \neq k} \sum_{l \neq m \neq n} X_{ijk} Y_{lmn} = \sum_{i \neq j \neq k \neq l \neq m \neq n} X_{ijk} Y_{lmn} + 9 \sum_{i \neq j \neq k \neq l \neq m} X_{ijk} Y_{klm} + 18 \sum_{i \neq j \neq k \neq l} X_{ijk} Y_{jkl} + 6 \sum_{i \neq j \neq k} X_{ijk} Y_{ijk} \quad (5.9)$$

for totally symmetric functions  $X$  and  $Y$ , with the symmetry factors derived by considering the number of possible ways to contract one, two or three pairs of indices from two sets of three. This allows Eq. 5.8 to be expressed in terms of three-, four-, five- and six-point functions and the order of index contractions is chosen for later use.

We must now consider the expansion of the six overdensity fields and their various contractions. For the sake of brevity, we combine terms with the same  $\{i, j, k\}$  and  $\{l, m, n\}$  permutation symmetries, since these all give identical contributions when we sum over all particles. The choice of index permutations shown have been chosen carefully for later convenience. From Wick's theorem

$$\begin{aligned} \langle \delta_i \delta_j \delta_k \delta_l \delta_m \delta_n \rangle_{\text{sym}} - \langle \delta_i \delta_j \delta_k \rangle \langle \delta_l \delta_m \delta_n \rangle &= (ijklmn) + 3(ij)(klmn) + 9(il)(jkmn) + 3(mn)(ijkl) \\ &+ 3(mn)(ijkl) + 9(ij)(klmn) + 9(ij)(kl)(mn) + 6(il)(jm)(kn) \\ \frac{n_k}{\alpha} \langle \delta_i \delta_j \delta_k \delta_l \delta_m \delta_k \rangle_{\text{sym}} = \langle (1 + \delta_k) \delta_i \delta_j \delta_l \delta_m \rangle_{\text{sym}} &= (ijklm) + (ijlm) + 2(ik)(jlm) + 2(kl)(ijm) + (ij)(klm) \\ &+ 4(il)(jkm) + (lm)(ijk) + (ij)(lm) + 2(il)(jm) \\ \frac{n_j n_k}{\alpha^2} \langle \delta_i \delta_j \delta_k \delta_l \delta_j \delta_k \rangle_{\text{sym}} = \langle (1 + \delta_i)(1 + \delta_j) \delta_k \delta_l \rangle &= (ijkl) + (il)(jk) + 2(ij)(kl) + 2(ijl) + (il) \\ \frac{n_i n_j n_k}{\alpha^3} \langle \delta_i \delta_j \delta_k \delta_i \delta_j \delta_k \rangle_{\text{sym}} = \langle (1 + \delta_i)(1 + \delta_j)(1 + \delta_k) \rangle &= (ijk) + 3(ij) + 1 \end{aligned} \quad (5.10)$$

denoting  $\xi_{x_1 \dots x_n}^{(n)}$  by  $(x_1 \dots x_n)$  as before and using the shot-noise contraction identity (Eq. 2.7). Inserting the above random field expansions into Eq. 5.8 and splitting into three- to six-point summations as in Eq. 5.9, we obtain the full solution for the 3PCF auto-covariance matrix;

$$\begin{aligned} C_{p,q}^{ab,cd} &= 6C_{p,q}^{ab,cd} + \alpha \times 5C_{p,q}^{ab,cd} + \alpha^2 \times 4C_{p,q}^{ab,cd} + \alpha^3 \times 3C_{p,q}^{ab,cd} \\ 6C_{p,q}^{ab,cd} &= \frac{(2p+1)(2q+1)}{\left[6V(\overline{nw})^3\right]^2} \sum_{i \neq j \neq k \neq l \neq m \neq n} n_i n_j n_k n_l n_m n_n w_i w_j w_k w_l w_m w_n K_{ijk}^{ab,p} K_{lmn}^{cd,q} \\ &\times \left[ \xi_{ijklmn}^{(6)} + 3 \xi_{ij} \xi_{klmn}^{(4)} + 9 \xi_{il} \xi_{jkmn}^{(4)} + 3 \xi_{mn} \xi_{ijkl}^{(4)} + 9 \xi_{ijl} \xi_{kmn} + 9 \xi_{ij} \xi_{kl} \xi_{mn} + 6 \xi_{il} \xi_{jm} \xi_{kn} \right] \\ 5C_{p,q}^{ab,cd} &= 9 \times \frac{(2p+1)(2q+1)}{\left[6V(\overline{nw})^3\right]^2} \sum_{i \neq j \neq k \neq l \neq m} n_i n_j n_k n_l n_m w_i w_j (w_k)^2 w_l w_m K_{ijk}^{ab,p} K_{klm}^{cd,q} \\ &\times \left[ \xi_{ijklm}^{(5)} + \xi_{ijlm}^{(4)} + 2 \xi_{ik} \xi_{jlm} + 2 \xi_{kl} \xi_{ijm} + \xi_{ij} \xi_{klm} + 4 \xi_{il} \xi_{jkm} + \xi_{lm} \xi_{ijk} + \xi_{ij} \xi_{lm} + 2 \xi_{il} \xi_{jm} \right] \\ 4C_{p,q}^{ab,cd} &= 18 \times \frac{(2p+1)(2q+1)}{\left[6V(\overline{nw})^3\right]^2} \sum_{i \neq j \neq k \neq l} n_i n_j n_k n_l w_i (w_j w_k)^2 w_l K_{ijk}^{ab,p} K_{jkl}^{cd,q} \\ &\times \left[ \xi_{ijkl}^{(4)} + 2 \xi_{ikl} + \xi_{il} \xi_{jk} + 2 \xi_{ij} \xi_{kl} + \xi_{il} \right] \\ 3C_{p,q}^{ab,cd} &= 6 \times \frac{(2p+1)(2q+1)}{\left[6V(\overline{nw})^3\right]^2} \sum_{i \neq j \neq k} n_i n_j n_k (w_i w_j w_k)^2 K_{ijk}^{ab,p} K_{ijk}^{cd,q} \\ &\times \left[ \xi_{ijk} + 3 \xi_{ij} + 1 \right] \end{aligned} \quad (5.11)$$

where we color the Gaussian terms in blue as before, noting Gaussian contributions to all terms. This may also be computed in  $\chi$ -bins ( $e, f$ ) rather than Legendre moments ( $p, q$ ), which has the same functional form, except that the  $K^{ab,p} K^{cd,q}$  kernels are replaced by  $\tilde{\Theta}^{ab,e} \tilde{\Theta}^{cd,f}$  binning functions (as in Eq. 4.4) and the prefactor changed to  $\left[RRR_e^{ab} RRR_f^{cd}\right]^{-1}$ .

### 5.2.2 Covariance Computation

Here we outline how the Gaussian contributions to the above 3PCF integral may be computed efficiently, via sampling sets of six spatial points ('hexes'), analogous to the quad-sampling algorithm introduced in [Philcox et al. \(2019\)](#) for the 2PCF auto-covariance. Although the integrals are of higher dimension than for the 2PCF, the use of Legendre polynomial bins and matrix compression (see Sec. 5.2.3) ensure that the number of bins is not too large, thus the matrices are relatively quick to converge. We begin by splitting up the Gaussian parts of Eqs. 5.11 into two distinct sets of summations giving

$$\begin{aligned}
6C_{p,q}^{ab,cd} &= 9 \sum_{i \neq j \neq k \neq l \neq m \neq n} \Omega_{ijk}^{ab,p} \Omega_{lmn}^{cd,q} [\xi_{ij} \xi_{kl} \xi_{mn}] + 6 \sum_{i \neq j \neq k \neq l \neq m \neq n} \Omega_{ijk}^{ab,p} \Omega_{lmn}^{cd,q} [\xi_{il} \xi_{jm} \xi_{kn}] \\
5C_{p,q}^{ab,cd} &= 9 \sum_{i \neq j \neq k \neq l \neq m} \Omega_{ijk}^{ab,p} \Omega_{klm}^{cd,q} [\xi_{ij} \xi_{lm}] + 18 \sum_{i \neq j \neq k \neq l \neq m} \Omega_{ijk}^{ab,p} \Omega_{klm}^{cd,q} [\xi_{il} \xi_{jm}] \\
4C_{p,q}^{ab,cd} &= 36 \sum_{i \neq j \neq k \neq l} \Omega_{ijk}^{ab,p} \Omega_{jkl}^{cd,q} [2\xi_{ij} \xi_{kl}] + 18 \sum_{i \neq j \neq k \neq l} \Omega_{ijk}^{ab,p} \Omega_{jkl}^{cd,q} [\xi_{il} \xi_{jk} + \xi_{il}] \\
3C_{p,q}^{ab,cd} &= 3 \sum_{i \neq j \neq k} \Omega_{ijk}^{ab,p} \Omega_{ijk}^{cd,q} [3\xi_{ij} + 1] + 3 \sum_{i \neq j \neq k \neq l} \Omega_{ijk}^{ab,p} \Omega_{ijk}^{cd,q} [3\xi_{jk} + 1],
\end{aligned} \tag{5.12}$$

using the definition

$$\Omega_{ijk}^{ab,p} = \frac{2p+1}{6V(nw)^3 v_a v_b} \times n_i n_j n_k w_i w_j w_k K_{ijk}^{ab,p}, \tag{5.13}$$

and noting that we have rewritten the  $18\xi_{ij}$  factor in the three-point term as  $9\xi_{ij} + 9\xi_{jk}$  (via interchange symmetry of the kernels and summations). These summations can simply be converted into integrals, e.g. replacing  $\sum_i$  with  $\int d^3 \mathbf{r}_i$ , and  $\xi_{ij}$  with  $\xi(\mathbf{r}_i - \mathbf{r}_j)$ . The two separate integral terms shown in Eq. 5.12 are henceforth labelled *A* and *B* and are computed separately. As detailed in Appendix A, the first of the six-point terms involves an integral over the full 2PCF  $\xi(\mathbf{r})$ , constrained only by the survey geometry, which should be zero for a uniform ideal survey. In reality, we do not expect perfect cancellation, but we expect the term to be small if the size of the survey is large compared with the BAO scale and maximum radial bin.

The two sets of terms may be computed by drawing sets of three to six points in three-dimensional space (subject to the survey selection functions) and computing the contribution of each to the relevant summations. For efficiency, we draw these points from an input set of random particle positions (such as those provided for clustering random counts), which naturally encode the survey number density distribution and mask. Integral convergence is greatly improved via importance sampling, where we preferentially sample points in space which have large contributions to the integral, and divide by the probability that that set of points was chosen. As in [Philcox et al. \(2019\)](#), we first assign particles to 'sampling cells', each of which contain a few particles, allowing us to pre-compute the probability that a particular cell is chosen. To draw a random particle from a given primary, we simply pick a secondary cell and choose a random particle representative from within.

Here, we consider two ways to draw a cell with center at  $r_a$  from one at  $r_b$ ; weighting by a  $|\mathbf{r}_a - \mathbf{r}_b|^{-2}$  kernel or by the isotropic 2PCF  $\xi(|\mathbf{r}_a - \mathbf{r}_b|)$ . The former is appropriate when we wish to fill up radial bins evenly (e.g. for two legs in the same triangle) whilst the latter is used for integrands containing the anisotropic term  $\xi_{ab}$  (although can also be used to fill radial bins since  $\xi \sim r^{-2}$  at leading order). The sampling probabilities using these two kernels are those given in [Philcox et al. \(2019, Sec. 3.4\)](#). The sampling strategy was tested by comparing the 2PCF-independent 3-point term to semi-analytic predictions in the uniform periodic limit, and found to be in excellent agreement across the binning ranges used here.

For both sets of integrals, we begin by drawing a single point from the set of random particles, then two more according to  $r^{-2}$  and  $\xi(r)$  kernels, and using these to compute the three-point integral contribution. Following this, a fourth particle is chosen from one of the previous particles via the  $\xi(r)$  kernel and used to compute the four-point integral contribution, which is then repeated for the five- and six-point terms, before the process is repeated. Since the higher-point integrals are expected to take longer to converge, we usually sample multiple quads of points from each triple, multiple quints (sets of five points) from each quad and multiple hexes from each quint. For a given set of points (which form two triangles), we compute the contributions to all pairs of Legendre moments  $p, q$  and all valid combinations of radial bins  $a, b, c, d$  (using the triangle kernel of Eq. 4.16). In Fig. 3 we describe diagrammatically the sampling strategies used to compute the two sets of integrals, showing the particle from which each subsequent particle is sampled, along with the choice of kernel. The exact ordering is carefully chosen to ensure that the integrals converge as quickly as possible.

### 5.2.3 Application to BOSS DR12 Mocks

To ensure that our theoretical 3PCF auto-covariance estimator is working correctly and to assess the validity of our shot-noise rescaling approximations, we must compare the output matrices to those from a suite of simulations. For this, we utilize QPM mocks appropriate for the BOSS DR12 surveys, as in Sec. 3.4. To form a sample covariance matrix, we first compute the 3PCF for each of 250 mocks using the algorithm of [Slepian & Eisenstein \(2015b\)](#), which has complexity  $\mathcal{O}(N^2)$  for  $N$  galaxies, and



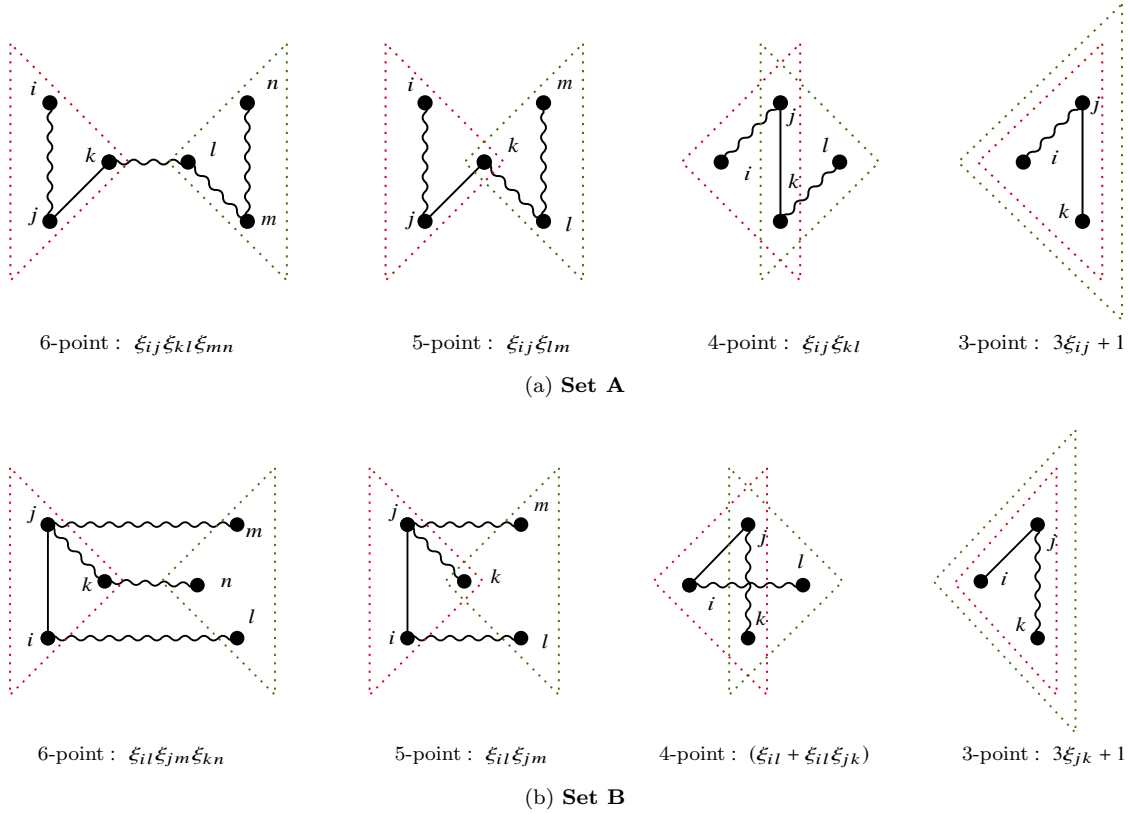


**Figure 3.** Pictorial representation of the sampling strategies used to compute the two sets of contributions to the 3PCF auto-covariance matrix integrals. The  $d$ -point covariance terms depend on  $d$  points in space (for  $d \in \{3, 4, 5, 6\}$ ); we here depict how these are chosen, as well as which term each configuration corresponds to. To compute the integrals we first draw three points in space,  $\{i, j, k\}$ , then add the  $l, m$  and  $n$  points successively to find a single contribution to each integral. Here a straight line indicates that a point is drawn from the previous via a  $1/r^2$  weighting (for separation  $r$ ), with a wavy line indicating a draw via an isotropic  $\xi(r)$  kernel. Each covariance integral depends on two triangles of points; the triplets of particles corresponding to each triangle are indicated by dashed lines.

incorporates the survey geometry via the multipoles of the  $RRR$  triple count. We adopt a binning strategy of  $\Delta r = 10h^{-1}\text{Mpc}$  up to a maximum radius of  $180h^{-1}\text{Mpc}$  (matching Slepian et al. 2015) using all Legendre multipoles up to  $\ell_{\max} = 6$ .  $\zeta_\ell$  multipoles are estimated as a ratio of  $NNN$  and  $RRR$  counts (cf. Eq. 4.1), requiring a large number of random galaxy positions to compute  $N = D - R$  counts (which involve significant cancellation), yet far fewer for the  $RRR$  counts, as noted in Slepian & Eisenstein (2015b). We follow the former paper’s approach of partitioning the random catalog into 32 random subsets, each with  $N_{\text{rand}} = 1.5N_{\text{gal}}$  particles, and averaging together the 32 resulting  $NNN$  counts, giving  $N_{\text{rand}} = 48N_{\text{gal}}$  in total. The  $RRR$  count is found to be well estimated using a single subset of randoms. For each QPM mock, 3PCF computation took  $\sim 2$  hours on 32 parallel CPUs, requiring a total of  $\sim 2 \times 10^4$  CPU-hours for the complete analysis.

For a reasonable choice of bin-width and  $\ell_{\max}$ , the total number of independent 3PCF bins (equal to  $N_r(N_r + 1)(\ell_{\max} + 1)/2$  for  $N_r$  radial bins) becomes large and hence difficult to interpret. To facilitate simpler visualization and covariance matrix comparison, we adopt the compression suggested by Slepian & Eisenstein (2015a) and Slepian et al. (2015), defining the compressed 3PCF,  $\zeta_{(c)}$ , as

$$\zeta_{(c),p}^a = \frac{\sum_{b \in S(a)} \zeta_p^{ab} v_b}{\sum_{b \in S(a)} v_b} \quad (5.14)$$

where  $v_b$  is the volume defined by (radial) bin  $b$  and  $S(a)$  is the set of all bins  $b$  satisfying  $3\Delta r \leq r_{b,\min} < r_{a,\min} - 3\Delta r$ , chosen to avoid the (strongly non-Gaussian) squeezed limit of the 3PCF. For the binning strategy described above, compression restricts utilized bins to  $r_b \geq 30h^{-1}\text{Mpc}$  and  $r_a \geq 70h^{-1}\text{Mpc}$  (since there are no  $b$  bins in  $S(a)$  for smaller  $r_a$ ), giving a total of 11 bins in the compressed 3PCF for each Legendre multipole, compared with  $15 \times 16/2 = 120$  in the uncompressed function. The resulting  $\zeta_{(c),p}^a$  measurements for the 250 QPM mocks are displayed in Fig. 5 and we note highly significant measurements of the  $\ell \geq 2$  multipoles for moderate  $r$ , indicating clear non-Gaussianity. These results are broadly consistent with the equivalent measurements for the MULTIDARK-PATCHY mocks (Kitaura et al. 2014; Kitaura 2014; Kitaura et al. 2015) presented in Slepian et al. (2015) for the same survey geometry.

Given the set of 250 compressed 3PCF estimates  $\{\hat{\zeta}_{(c),p}^{(n),a}\}$  with mean  $\bar{\zeta}_{(c),p}^a$ , the compressed covariance (denoted by  $\mathbb{C}$ ) is

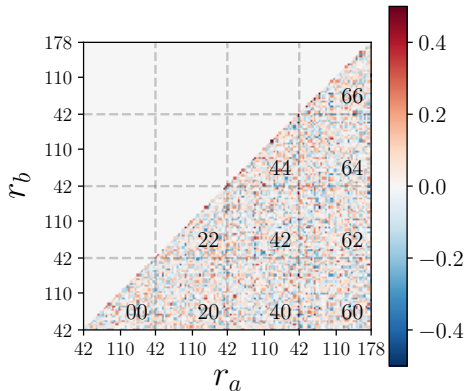


**Figure 4.** Discriminant matrix  $\mathbf{P}$  between theoretical and sample covariance matrices of the anisotropic 2PCF in Legendre bins, defined in Eq. 3.31. The theoretical matrix is displayed in reduced form in Fig. 2, with the sample matrix being constructed from angularly-binned 2PCF estimates from 99 QPM mocks, as shown in Fig. 1. Pairs of multipoles are indicated by the text, as in Fig. 2, and we note that  $\mathbf{P}$  is zero for identical matrices in the absence of noise. Since the matrix is symmetric by definition, we only show the lower diagonal, to avoid spurious correlations being observed due to the symmetry. As described in Sec. 3.4, the difference between the matrices appears to be solely consistent with noise at this resolution level.

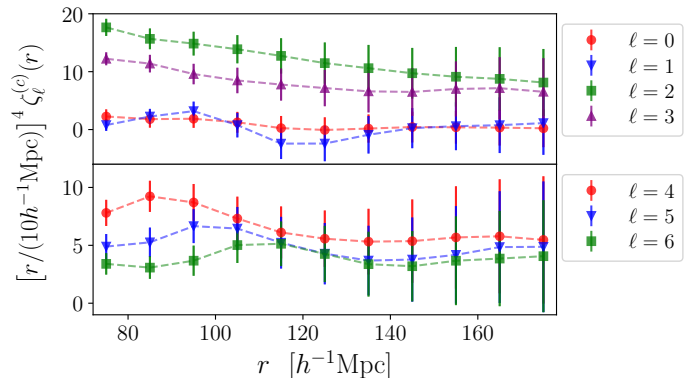


**Figure 5.** Compressed three-point correlation function (3PCF) multipoles measured from 250 BOSS DR12 Quick Particle Mesh (QPM; White et al. 2014) mocks using the  $O(N^2)$  algorithm of Slepian & Eisenstein (2015b). The 3PCF is measured from  $\sim 6 \times 10^5$  galaxies in each mock, using the Szapudi & Szalay (1998) estimator to correct for boundary effects, and the compression of Slepian & Eisenstein (2015a) to convert the 3PCF to a set of one-dimensional functions, averaging over radial bins which avoid the (non-Gaussian) squeezed limit. Error bars represent the standard deviation of the 250 measurements and are not normalized by  $\sqrt{N_{\text{mocks}}}$ , i.e. they represent the precision possible from a single galaxy survey. There is a highly significant measurement of non-Gaussianity at smaller scales and we note broad consistency with the 3PCF measurements of Slepian et al. (2015), computed for the MULTI-DARK PATCHY BOSS DR12 simulations. These measurements are used to compute the 3PCF covariances of Sec. 5.2.3.

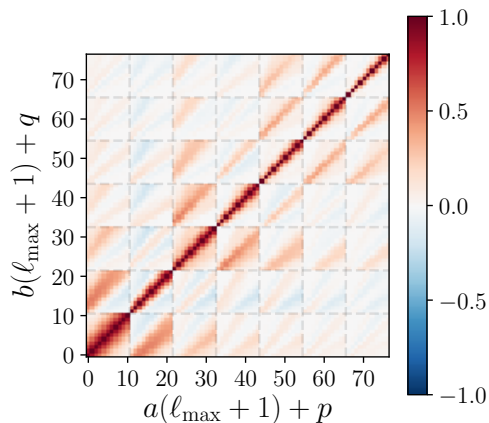


**Figure 6.** Theoretical correlation matrix (Eq. 3.28) for the compressed isotropic 3PCF measurements presented in Fig. 5 for the BOSS DR12 CMASS-N geometry. This is computed using the newly-extended `RascalC` code in  $\sim 200$  CPU-hours, with a numerical noise-level comparable to that of  $2 \times 10^4$  mocks. The compressed matrix is related to the full 3PCF covariance by Eq. 5.16. This is analogous to Fig. 2, except that we now use the 3PCF and display data for both odd and even Legendre multipoles, from  $(p, q) = (0, 0)$  (lower left) to  $(6, 6)$  (upper right). Each multipole pair inhabits its own submatrix, with the radial bin indices  $a, b$  running from 0 to 10, denoting linear bins from  $r = 70 - 80h^{-1}\text{Mpc}$  to  $r = 170 - 180h^{-1}\text{Mpc}$ . To encapsulate some degree of non-Gaussianity, we have included a shot-noise rescaling parameter of  $\alpha = 1.20$ , calibrated by minimizing the Kullback-Leibler (Kullback & Leibler 1951) divergence between the noisy sample matrix and the smooth theoretical matrix. We note strong positive correlations between bins with the same multipole, with significant negative correlations when  $p$  or  $q$  is odd.

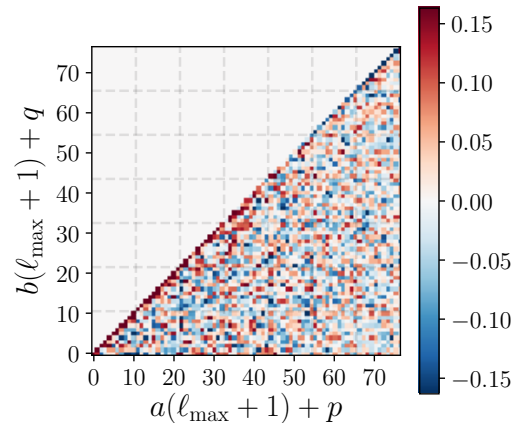


**Figure 7.** Discriminant matrix between sample and theoretical compressed 3PCF covariance matrices, as defined in Eq. 3.31. The reduced theoretical matrix is shown in Fig. 6 (in the same format as here) and the sample matrix is constructed from the covariance of 250 compressed 3PCF measurements, which are shown in Fig. 5. As in Fig. 4, we mask the upper half of the matrix to avoid spurious correlations being observed from symmetry. If the theoretical matrix matches the data, we expect the discriminant matrix to be consistent with zero; as noted in the text, there is a slight excess of root-mean-square deviation here, concentrated along the leading diagonal. This indicates some small differences between sample and theoretical matrices, most likely due to the lack of proper inclusion of non-Gaussianity terms in our model.

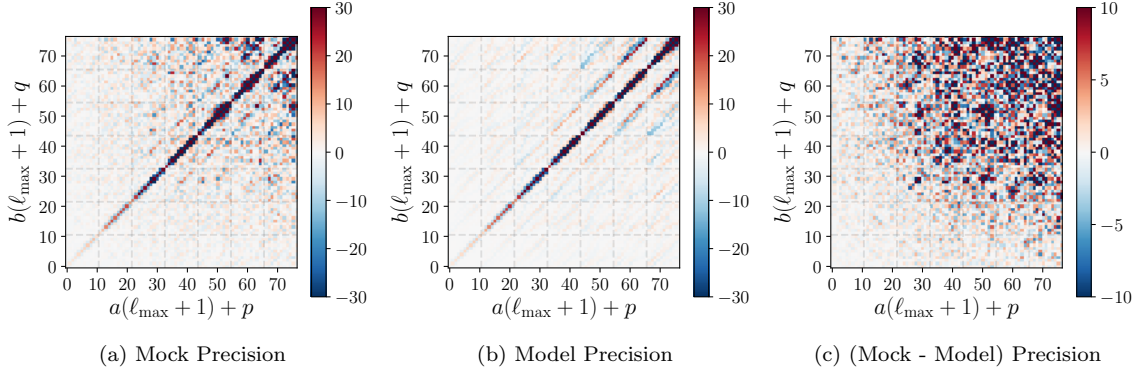


**Figure 8.** Comparison of the sample and theoretical compressed 3PCF precision matrices across a number of radial bins and Legendre moments, in the same format as Figs. 6 & 7, again using a theoretical shot-noise rescaling parameter of  $\alpha = 1.20$ . The sample (theoretical) compressed precision matrix is defined by Eq. 3.29 (3.30) and we remove the leading scalings by multiplying by  $(2p+1)(2q+1)/(r_a r_b)^2$ . We do not notice any systematic differences between the matrices except for larger noise at high multipole moment, as expected since the higher multipoles become significantly more noisy. An alternative comparison between the matrices is presented in Fig. 7.

defined in the standard manner;

$$\mathbb{C}_{p,q}^{a,b} = \frac{1}{N_{\text{mocks}} - 1} \sum_{n=1}^{N_{\text{mocks}}} \left[ \left( \zeta_{(c),p}^{(n),a} - \bar{\zeta}_{(c),p}^a \right) \left( \zeta_{(c),q}^{(n),b} - \bar{\zeta}_{(c),q}^b \right) \right], \quad (5.15)$$

and is related to the uncompressed covariance by

$$\mathbb{C}_{p,q}^{a,b} = \frac{\sum_{c \in \mathcal{S}(a)} \sum_{d \in \mathcal{S}(b)} \mathbb{C}_{p,q}^{ac,bd} v_c v_d}{\sum_{c \in \mathcal{S}(a)} \sum_{d \in \mathcal{S}(b)} v_c v_d} \quad (5.16)$$

where  $\mathbb{C}_{p,q}^{ac,bd} = \text{cov}(\zeta_p^{ac}, \zeta_q^{bd})$ . The (symmetric) compressed matrix has a total of  $\frac{1}{2} [N_r^{(c)}(\ell_{\text{max}} + 1)] [(N_r^{(c)}(\ell_{\text{max}} + 1) + 1)] = 3003$  independent components, where  $N_r^{(c)} = 11$  is the number of radial bins allowed by the compression strategy. In contrast, the uncompressed matrix has  $\frac{1}{2} N_{\text{elem}}(N_{\text{elem}} + 1)$  elements, for  $N_{\text{elem}} = \frac{1}{2} N_r(N_r + 1)(\ell_{\text{max}} + 1)$ , or greater than  $10^6$  for  $N_r = 15$ . The large reduction in dimensionality provided by the compression thus significantly reduces matrix noise and gives much expedited integral convergence.

The theoretical compressed covariance is computed via the algorithm discussed in Sec. 5.2.2, initially computing the fully symmetric matrix  $\mathbb{C}_{p,q}^{ab,cd}$  before applying the compression of Eq. 5.16. The relevant three- to six-point integrals are sampled using positions taken from a  $N_{\text{rand}} = 10N_{\text{gal}}$  random catalog, with an additional input being a finely binned 2PCF estimated from the mean of 1000 QPM mocks, as in Sec. 3.4. To determine the three-point survey-correction function  $\Phi(r_a, r_b, \chi)$ , we first compute the *RRR* triple counts of a small random catalog, using the output monopoles to define a smooth function (via Eq. 4.10), which is additionally normalized by  $6V(nw)^3$  for later convenience. For any given pair of bins, we found the inverse function  $\Phi^{-1}(r_a, r_b, \chi)$  to be well fit by its first six multipoles, allowing for quick reconstruction when the code is run (noting that the relevant Legendre polynomials already must be computed by the sampler). In total, we sample  $8.4 \times 10^{12}$  hexes of particles (including those rejected for being outside the survey or in incorrect bins) over 260 CPU-hours (with trivial parallelization possible). For a given number of hexes sampled, the computation time scales as  $(\ell_{\text{max}} + 1)^2$ , since we must add each accepted set to this many Legendre bins.

Since the width of the DR12 survey ( $\sim 1600h^{-1}\text{Mpc}$ ) is large compared to the characteristic scale of  $\xi(\mathbf{r})$  ( $\sim 100h^{-1}\text{Mpc}$ ) and the maximum bin-size ( $180h^{-1}\text{Mpc}$ ), we expect the first six-point covariance term to be strongly subdominant compared with the other terms (see Appendix A). Computationally, this term poses difficulties, since cancellation occurs via negative contributions at large radius balancing positive ones at small  $r$ . Accurate computation of this term requires sampling of all possible values of the  $k-l$  particle separation (cf. Fig. 3) which is inefficient, thus we here simply assume the term to be zero.

An important hyperparameter in our theoretical covariance matrix is the shot-noise rescaling parameter  $\alpha$ , used to approximate non-Gaussianity. In previous work (O’Connell & Eisenstein 2019; Philcox et al. 2019) it was shown that, for the 2PCF, this could be constrained via splitting the survey into jackknife regions and comparing theoretical and jackknife covariance matrices. Whilst this remains possible for the 3PCF, we here adopt a simpler approach, computing  $\alpha$  by fitting the theoretical to sample covariance matrix. Although this introduces dependence of our theoretical matrix on mock data, we note that we do not need a large number of mocks to constrain  $\alpha$ , since there is only a single degree of freedom. As before,  $\alpha$

is determined by minimizing the Kullback-Leibler (Kullback & Leibler 1951) divergence between the matrices;

$$\begin{aligned}\alpha^* &= \arg \min_{\alpha} [D_{KL}(\hat{\Psi}_{\text{theory}}(\alpha), \hat{\mathbf{C}}_{\text{sample}})] \\ D_{KL}(\Psi, \mathbf{C}) &= \frac{1}{2} [\text{trace}(\Psi\mathbf{C}) - \log \det \Psi - \log \det \mathbf{C} - N_{\text{bins}}].\end{aligned}\tag{5.17}$$

We obtain an optimal value of  $\alpha = 1.20$ , significantly larger than that of the 2PCF (1.032) indicating that non-Gaussianity is more important in the 3PCF auto-covariance. Using  $N_{\text{samples}} = 40$  individual matrix estimates (each run on a different core) with this shot-noise rescaling, we obtain  $N_{\text{eff}} = 2 \times 10^4$  from Eq. 3.31, implying that our co-added estimate has a precision comparable with that of 20,000 mocks. Despite sampling the same number of particle sets as for the 2PCF auto-covariance in Sec. 3.4, we note a much reduced  $N_{\text{eff}}$ ; this is due to the higher dimensionality of our problem; sampling in 18-dimensions naturally gives slower convergence than 12-dimensions. We further note that  $N_{\text{eff}}$  scales linearly with the number of hexes sampled, thus greater precision (though not necessarily accuracy) can be obtained simply via longer integration time.

The resulting compressed 3PCF correlation matrix (defined analogously to the 2PCF case of Eq. 3.28) is displayed in Fig. 6. Strongest correlations are seen between bins with the same multipole moment (i.e.  $p = q$ ), though these are still non-negligible for bins with very different multipole moments. Noticeably, correlations involving odd multipoles are negative away from the leading diagonal and there is strong correlation of all bins with the quadrupole term, which is seen to be the dominant non-Gaussian component in Fig. 5.

A simple way to compare theory to simulation is via the precision matrices (computed via Eqs. 3.29 & 3.30), which are plotted in Fig. 8. We choose to plot these rather than the covariance matrices since they have more relevance for parameter inference, though we require a large  $N_{\text{mocks}}$  to ensure invertibility (which is why the 2PCF sample precision was not shown in Sec. 3.4). Plotting the matrices multiplied by  $(2p+1)(2q+1)/(r_a r_b)^2$  to remove the leading scalings, we note good agreement between mock and model precision for low multipoles, with significant random error in the mock data for higher  $(p, q)$  pairs, due to the greater intrinsic noise in these 3PCF measurements. Indeed, plotting the difference of sample and theoretical covariance matrices (Fig. 8c) shows no noticeable systematic differences between the two, although we are strongly noise limited at larger  $(p, q)$ . More mocks are required to further constrain systematic differences between the precision matrices.

As in Sec. 3.4, we may additionally compare matrices via the discriminant matrix,  $\mathbf{P}$ , defined in Eq. 3.31 and displayed in Fig. 7. Although the bulk of the matrix appears consistent with random fluctuations, there is a slight overestimate along the diagonal (where  $a = b$  and  $p = q$ ), which indicates some systematic differences between matrices. The mean and root-mean-square of  $\mathbf{P}$  are here found to be 0.13% and 5.8% respectively, compared to the expected deviance of 4.9% given the number of degrees of freedom and  $N_{\text{mocks}}$ , which again indicates a slight bias. This difference is attributed to the lack of proper inclusion of non-Gaussian terms in our 3PCF covariance formalism and may be significantly reduced via simple models for the 3PCF, e.g. hierarchical models (Peebles & Groth 1975; Groth & Peebles 1977). However, the lack of any noticeable features in the precision matrix differential indicates that this may not have major impacts for cosmological analyses.

Holistically, it is clear that our 3PCF covariance matrix formalism is able to produce useful estimates for the survey-dependent 3PCF auto-covariance matrix which are in fair agreement with those from a suite of mocks, especially when considering the precision matrices. The success of our shot-noise rescaled estimates is perhaps surprising, given recent works such as Chan & Blot (2017), which claim that the non-Gaussian contributions to the 3PCF covariance are large even on mildly non-linear scales. We note however that (a) we require a larger shot-noise rescaling for the 3PCF than the 2PCF auto-covariance, indicating more non-Gaussianity, and (b) we have focused on scales above  $40 h^{-1} \text{Mpc}$  (as appropriate for BAO analyses), where the effects of non-Gaussianity are expected to be weak. We expect our approximation to lose accuracy on small scales.

## 6 SUMMARY AND OUTLOOK

In this paper we have developed a formalism for estimating theoretical anisotropic two-point and isotropic three-point correlation function covariance matrices in Legendre multipole bins for arbitrary survey geometries, extending the work of O’Connell et al. (2016), O’Connell & Eisenstein (2019) and Philcox et al. (2019). Our covariances have been derived in configuration space via shot-noise expansions and Wick contractions of the density field, giving a set of integrals from which the Gaussian covariance can be estimated. To incorporate Legendre multipoles, we introduced a model for the random pair or triple counts and an associated geometry-correction function, which allowed us to sample Legendre covariances directly, rather than constructing them from angularly binned covariances in post-processing. As in previous works, a shot-noise rescaling parameter was included to account for some non-Gaussianity; this may be calibrated either from a (small) set of mocks or jackknives and allows us to neglect higher order terms in the matrix expansion.

We have extended the previously used 2PCF algorithm to the new cases considered here, estimating the relevant integrals by sampling sets of two to six points in space, made highly efficient via importance sampling and careful ordering of terms.

This has been incorporated into the publicly available `RascalC` code,<sup>5</sup> giving 2PCF (3PCF) covariance matrices with negligible sampling noise in  $\sim 10$  ( $\sim 100$ ) CPU-hours for BOSS-like surveys. We demonstrated the accuracy of our estimates by comparison with sample covariance matrices derived from Quick Particle Mesh mocks appropriate for BOSS DR12 (which are computed at much larger computational expense). For the 2PCF we found excellent agreement between theory and simulations, with only a small bias found in the 3PCF matrices, though this was not found to have a noticeable impact on the precision matrices. We caution that we do not expect such good agreement between shot-noise rescaled theory and mocks on significantly smaller scales.

We expect that any differences between theoretical and sample matrices may be substantially reduced by including the 3PCF in our covariance integrals, either through some simple model, or as a fit to the measured data. A simple way to achieve this would be through hierarchical models (Peebles & Groth 1975; Groth & Peebles 1977), where the 3PCF is written as  $\zeta(\mathbf{r}_1, \mathbf{r}_2) = Q[\xi(r_1)\xi(r_2) + \xi(r_1)\xi(|\mathbf{r}_1 - \mathbf{r}_2|) + \xi(r_2)\xi(|\mathbf{r}_1 - \mathbf{r}_2|)]$ , for hierarchical parameter  $Q$ . Although it is well known that  $Q$  varies as a function of triangle configuration (e.g. Takada & Jain 2003), fitting for a constant  $Q$  will allow for a more accurate inclusion of non-Gaussianity, though at the expense of significant additional computation time for the 3PCF matrices.

The isotropic 3PCF covariance integrals presented herein may be simply extended to the anisotropic case, which involves an additional two 3PCF parameters describing the orientation of a triangle with respect to the mean line of sight, allowing for proper inclusion of redshift space distortion effects. This will modify the integrals only by the insertion of additional orientation-dependent binning functions (or Legendre multipoles), but we note that both the anisotropic 3PCF and its covariance are difficult to visualize, due to their high dimensionality. In addition, without some suitable compression, the number of independent bins is large, leading to slow convergence of the output matrices. An additional extension is to the cross-covariance of the correlation functions with the power-spectrum; this will be discussed in future work.

The benefit provided by algorithms for approximate covariance matrix generation is many-fold; due to the approaches' smaller dependence on mocks, computational focus can be shifted towards creating a few high accuracy mocks, rather than a large number, simply to drive down sample covariance matrix noise. In addition, the vast speed boost allows for new avenues of exploration, such as full analyses of the dependence of covariances on the survey geometry and assumed cosmology, which are infeasible using conventional mock-based approaches. It is the hope of both authors that the approaches presented in this paper will be used in future analyses of survey data (especially those applying multiple statistics in concert) to compute high precision covariances at low computational effort, and therefore assist in placing strong constraints on cosmological parameters.

## ACKNOWLEDGEMENTS

We thank the referee for insightful comments helping to improve the clarity of this paper. OHEP acknowledges funding from the Herchel-Smith foundation. DJE is supported by U.S. Department of Energy grant DE-SC0013718 and as a Simons Foundation Investigator.

Some of the computations in this paper were run on the Odyssey cluster supported by the FAS Division of Science, Research Computing Group at Harvard University. Funding for SDSS-III has been provided by the Alfred P. Sloan Foundation, the Participating Institutions, the National Science Foundation, and the U.S. Department of Energy Office of Science. The SDSS-III web site is [www.sdss3.org/](http://www.sdss3.org/).

SDSS-III is managed by the Astrophysical Research Consortium for the Participating Institutions of the SDSS-III Collaboration including the University of Arizona, the Brazilian Participation Group, Brookhaven National Laboratory, Carnegie Mellon University, University of Florida, the French Participation Group, the German Participation Group, Harvard University, the Instituto de Astrofísica de Canarias, the Michigan State/Notre Dame/JINA Participation Group, Johns Hopkins University, Lawrence Berkeley National Laboratory, Max Planck Institute for Astrophysics, Max Planck Institute for Extraterrestrial Physics, New Mexico State University, New York University, Ohio State University, Pennsylvania State University, University of Portsmouth, Princeton University, the Spanish Participation Group, University of Tokyo, University of Utah, Vanderbilt University, University of Virginia, University of Washington, and Yale University.

## REFERENCES

- Alam S., et al., 2015, *The Astrophysical Journal Supplement Series*, **219**, 12  
 Alam S., et al., 2017, *MNRAS*, **470**, 2617  
 Alcock C., Paczynski B., 1979, *Nature*, **281**, 358  
 Bernardeau F., Colombi S., Gaztañaga E., Scoccimarro R., 2002, *Phys. Rep.*, **367**, 1  
 Bernstein G. M., 1994, *ApJ*, **424**, 569  
 Chan K. C., Blot L., 2017, *Phys. Rev. D*, **96**, 023528

<sup>5</sup> [RascalC.readthedocs.io](https://github.com/DMDE/rascalC.readthedocs.io)



- DESI Collaboration et al., 2016, arXiv e-prints, p. [arXiv:1611.00036](https://arxiv.org/abs/1611.00036)
- Dawson K. S., et al., 2013, *AJ*, **145**, 10
- Desjacques V., Seljak U., 2010, *Classical and Quantum Gravity*, **27**, 124011
- Eisenstein D. J., et al., 2011, *AJ*, **142**, 72
- Feldman H. A., Kaiser N., Peacock J. A., 1994, *ApJ*, **426**, 23
- Frieman J. A., Gaztanaga E., 1994, *ApJ*, **425**, 392
- Gardner J. P., Connolly A., McBride C., 2007, arXiv e-prints, p. [arXiv:0709.1967](https://arxiv.org/abs/0709.1967)
- Gaztanaga E., Frieman J. A., 1994, *ApJ*, **437**, L13
- Gray A. G., Moore A. W., Nichol R. C., Connolly A. J., Genovese C., Wasserman L., 2004, in Ochsenbein F., Allen M. G., Egret D., eds, *Astronomical Society of the Pacific Conference Series Vol. 314, Astronomical Data Analysis Software and Systems (ADASS) XIII*, p. 249 ([arXiv:astro-ph/0401121](https://arxiv.org/abs/astro-ph/0401121))
- Groth E. J., Peebles P. J. E., 1977, *ApJ*, **217**, 385
- Guo H., et al., 2015, *MNRAS*, **449**, L95
- Hartlap J., Simon P., Schneider P., 2007, *A&A*, **464**, 399
- Isserlis L., 1918, *Biometrika*, **12**, 134
- Jackson J. C., 1972, *MNRAS*, **156**, 1P
- Jing Y. P., Börner G., 2004, *ApJ*, **607**, 140
- Kaiser N., 1987, *MNRAS*, **227**, 1
- Kayo I., et al., 2004, *PASJ*, **56**, 415
- Kazin E. A., Sánchez A. G., Blanton M. R., 2012, *MNRAS*, **419**, 3223
- Kitaura F.-S., 2014, arXiv e-prints, p. [arXiv:1405.6273](https://arxiv.org/abs/1405.6273)
- Kitaura F. S., Yepes G., Prada F., 2014, *MNRAS*, **439**, L21
- Kitaura F.-S., Gil-Marín H., Scóccola C. G., Chuang C.-H., Müller V., Yepes G., Prada F., 2015, *MNRAS*, **450**, 1836
- Kullback S., Leibler R. A., 1951, *Ann. Math. Statist.*, **22**, 79
- Landy S. D., Szalay A. S., 1993, *ApJ*, **412**, 64
- Laureijs R., et al., 2011, arXiv e-prints, p. [arXiv:1110.3193](https://arxiv.org/abs/1110.3193)
- Levi M., et al., 2013, arXiv e-prints, p. [arXiv:1308.0847](https://arxiv.org/abs/1308.0847)
- Marín F., 2011, *ApJ*, **737**, 97
- Marín F. A., Wechsler R. H., Frieman J. A., Nichol R. C., 2008, *ApJ*, **672**, 849
- Moore A. W., et al., 2001, in Banday A. J., Zaroubi S., Bartelmann M., eds, *Mining the Sky*. p. 71 ([arXiv:astro-ph/0012333](https://arxiv.org/abs/astro-ph/0012333)), [doi:10.1007/10849171\\_5](https://doi.org/10.1007/10849171_5)
- Nichol R. C., et al., 2006, *MNRAS*, **368**, 1507
- O’Connell R., Eisenstein D. J., 2019, *MNRAS*, **487**, 2701
- O’Connell R., Eisenstein D., Vargas M., Ho S., Padmanabhan N., 2016, *MNRAS*, **462**, 2681
- Peacock J. A., et al., 2001, *Nature*, **410**, 169
- Peebles P. J. E., Groth E. J., 1975, *ApJ*, **196**, 1
- Percival W. J., et al., 2014, *MNRAS*, **439**, 2531
- Philcox O. H. E., Eisenstein D. J., O’Connell R., Wiegand A., 2019, arXiv e-prints, p. [arXiv:1904.11070](https://arxiv.org/abs/1904.11070)
- Sánchez A. G., et al., 2017, *MNRAS*, **464**, 1640
- Satpathy S., et al., 2017, *MNRAS*, **469**, 1369
- Scoccimarro R., Zaldarriaga M., Hui L., 1999, *ApJ*, **527**, 1
- Sefusatti E., Crocce M., Pueblas S., Scoccimarro R., 2006, *Phys. Rev. D*, **74**, 023522
- Sinha M., Garrison L., 2017, Corrfunc: Blazing fast correlation functions on the CPU ([ascl:1703.003](https://arxiv.org/abs/ascl:1703.003))
- Slepian Z., Eisenstein D. J., 2015a, *MNRAS*, **448**, 9
- Slepian Z., Eisenstein D. J., 2015b, *MNRAS*, **454**, 4142
- Slepian Z., Eisenstein D. J., 2017, *MNRAS*, **469**, 2059
- Slepian Z., Eisenstein D. J., 2018, *MNRAS*, **478**, 1468
- Slepian Z., et al., 2015, arXiv e-prints, p. [arXiv:1512.02231](https://arxiv.org/abs/1512.02231)
- Slepian Z., et al., 2017, *MNRAS*, **469**, 1738
- Slepian Z., et al., 2018, *MNRAS*, **474**, 2109
- Spergel D., et al., 2015, arXiv e-prints, p. [arXiv:1503.03757](https://arxiv.org/abs/1503.03757)
- Sugiyama N. S., Saito S., Beutler F., Seo H.-J., 2019, arXiv e-prints, p. [arXiv:1908.06234](https://arxiv.org/abs/1908.06234)
- Szapudi I., 2004, *ApJ*, **605**, L89
- Szapudi I., 2005, arXiv e-prints, [pp astro-ph/0505391](https://arxiv.org/abs/astro-ph/0505391)
- Szapudi I., Szalay A. S., 1998, *ApJ*, **494**, L41
- Takada M., Jain B., 2003, *MNRAS*, **340**, 580
- Taylor A., Joachimi B., Kitching T., 2013, *MNRAS*, **432**, 1928
- Vargas-Magaña M., et al., 2018, *MNRAS*, **477**, 1153
- White M., Tinker J. L., McBride C. K., 2014, *MNRAS*, **437**, 2594
- Wishart J., 1928, *Biometrika*, **20A**, 32
- Xu X., et al., 2010, *ApJ*, **718**, 1224
- Yuan S., Eisenstein D. J., Garrison L. H., 2017, *MNRAS*, **472**, 577
- Yuan S., Eisenstein D. J., Garrison L. H., 2018, *MNRAS*, **478**, 2019
- Zarrouk P., et al., 2018, *MNRAS*, **477**, 1639
- Zhang L. L., Pen U.-L., 2005, *New Astron.*, **10**, 569



**APPENDIX A: CANCELLING TERM IN THE 3PCF AUTO-COVARIANCE**

We here discuss the cancellation of the first Gaussian six-point term in the theoretical 3PCF auto-covariance expansion. From Eq. 5.11, we may write the first Gaussian term in integral form as

$$\begin{aligned}
 {}_A^6 C_{p,q}^{ab,cd} &= 9 \frac{(2p+1)(2q+1)}{\left[6V(nw)^3\right]^2 v_a v_b v_c v_d} \int d^3 \mathbf{r}_i d^3 \mathbf{r}_j d^3 \mathbf{r}_k d^3 \mathbf{r}_l d^3 \mathbf{r}_m d^3 \mathbf{r}_n n(\mathbf{r}_i) n(\mathbf{r}_j) n(\mathbf{r}_k) n(\mathbf{r}_l) n(\mathbf{r}_m) n(\mathbf{r}_n) \\
 &\times w(\mathbf{r}_i) w(\mathbf{r}_j) w(\mathbf{r}_k) w(\mathbf{r}_l) w(\mathbf{r}_m) w(\mathbf{r}_n) K^{ab,p}(\mathbf{r}_i, \mathbf{r}_j, \mathbf{r}_k) K^{cd,q}(\mathbf{r}_l, \mathbf{r}_m, \mathbf{r}_n) \xi(\mathbf{r}_i - \mathbf{r}_j) \xi(\mathbf{r}_k - \mathbf{r}_l) \xi(\mathbf{r}_m - \mathbf{r}_n) \\
 &= \int d^3 \mathbf{r}_k d^3 \mathbf{r}_l \mathcal{H}^{ab,p}(\mathbf{r}_k) \mathcal{H}^{cd,q}(\mathbf{r}_l) \xi(\mathbf{r}_k - \mathbf{r}_l)
 \end{aligned} \tag{A1}$$

where we have separated out the integrals over  $\mathbf{r}_k$  and  $\mathbf{r}_l$  and defined the partial integral

$$\begin{aligned}
 \mathcal{H}^{ab,p}(\mathbf{r}_j) &= \frac{2p+1}{2V(nw)^3 v_a v_b} \int d^3 \mathbf{r}_i d^3 \mathbf{r}_k n(\mathbf{r}_i) n(\mathbf{r}_k) w(\mathbf{r}_i) w(\mathbf{r}_k) K^{ab,p}(\mathbf{r}_i, \mathbf{r}_j, \mathbf{r}_k) \xi(\mathbf{r}_i - \mathbf{r}_j) \\
 &= \frac{2p+1}{2V(nw)^3} \int d^3 \mathbf{r}_i d^3 \mathbf{r}_j n(\mathbf{r}_i) n(\mathbf{r}_j) w(\mathbf{r}_i) w(\mathbf{r}_j) \xi(\mathbf{r}_i - \mathbf{r}_j) \left[ \Theta^a(\mathbf{r}_i - \mathbf{r}_j) \Theta^b(\mathbf{r}_i - \mathbf{r}_k) \Phi(r_a, r_b, \chi(\mathbf{r}_j - \mathbf{r}_k)) L_p(\chi(\mathbf{r}_j - \mathbf{r}_k)) + 5 \text{ perms.} \right]
 \end{aligned} \tag{A2}$$

(expanding  $K^{ab,p}$  in the second line) with an analogous form for  $\mathcal{H}^{cd,q}(\mathbf{r}_k)$ . Notably,  $\mathcal{H}$  is simply a (weighted) integral of the 2PCF and a Legendre polynomial over all triangles with sides in bins  $a, b$ , with  $\mathbf{r}_k$  specifying the position of one of the triangle vertices. For an ideal uniform survey with periodic boundary conditions, we would expect this integral to be invariant under spatial translations of the triangle, thus  $\mathcal{H}(\mathbf{r}_k)$  should be independent of  $\mathbf{r}_k$ . In this limit, the covariance term may be simplified as

$${}_A^6 C_{p,q}^{ab,cd} = \mathcal{H}^{ab,p} \mathcal{H}^{cd,q} \int d^3 \mathbf{r}_k d^3 \mathbf{r}_l \xi(\mathbf{r}_k - \mathbf{r}_l) = \mathcal{H}^{ab,p} \mathcal{H}^{cd,q} \times V \int d^3 \mathbf{r}_{kl} \xi(\mathbf{r}_{kl}) \tag{A3}$$

transforming  $\mathbf{r}_k$  to  $\mathbf{r}_{kl} \equiv \mathbf{r}_k - \mathbf{r}_l$  and integrating over the survey volume  $V$ . Noting that the 2PCF is defined as an over-random probability, we expect its infinite integral to be zero, such that the large-scale mean galaxy number density is equal to the density in the absence of correlations. In practice, we are limited by the finite volume of the survey and the lack of knowledge of the true uncorrelated number density, but the 2PCF integral (equal to the zero-momentum power spectrum  $P(\mathbf{0})$ ) is expected to be small.

For a realistic survey, we will expect some dependence of  $\mathcal{H}$  on position (due to boundaries and non-uniform number densities and weights) but, assuming the characteristic survey size  $L$  is much larger than the maximum bin-width, this dependence is expected to be weak. Furthermore, if  $L$  is large compared to the characteristic scale of  $\xi(\mathbf{r})$  (i.e. the BAO scale  $\sim 100 h^{-1} \text{Mpc}$ ) the 2PCF integral will be small, thus the entire term is expected to be negligible compared to the other six-point covariance integral, for all combinations of bins and Legendre moments.

This paper has been typeset from a  $\text{\TeX}/\text{\LaTeX}$  file prepared by the author.